

Article

Spatiotemporal Variation of Summertime Urban Heat Island (UHI) and Its Correlation with Particulate Matter (PM_{2.5}) over Metropolitan Cities in Alabama

Gamal El Afandi *  and Hossam Ismael 

College of Agriculture, Environment and Nutrition Sciences, Tuskegee University, Tuskegee, AL 36088, USA; hismael@tuskegee.edu

* Correspondence: gelafandi@tuskegee.edu; Tel.: +1-334-724-4790

Abstract: More than half of the global population lives in urban areas, which can cause the phenomenon known as Urban Heat Island (UHI). UHI is a phenomenon where urban areas experience higher temperatures compared to their rural surroundings. The occurrence of UHI in large cities is primarily due to urbanization and increased vehicular emissions. Factors such as wind speed and direction, solar flux, and the thermodynamic properties of surface materials determine the intensity of UHI. It can cause thermal air circulation, leading to high concentrations of urban air pollutants such as fine particulate matter (PM_{2.5}). These pollutants can remain suspended in the air and cause asthma and allergies. It is essential to understand the characteristics of UHI intensity and its effect on air quality. This study aims to analyze the spatiotemporal variations of UHI and their correlation with PM_{2.5} concentration in three Alabama cities, namely Birmingham, Montgomery, and Mobile, during the summer seasons of 2002, 2012, and 2022. The study also compares UHI in these cities with nearby rural areas to determine the effect of urbanization by calculating the Normalized Difference Building Index (NDBI). To achieve these objectives, the Land Surface Temperature (LST), UHI intensity, and NDBI Datasets were analyzed. The results showed that PM_{2.5} concentrations in the cities have been decreasing annually since 2002, leading to an improvement in air quality. There was a negative linear correlation between UHI intensity and PM_{2.5} concentration. However, LST remained consistently high throughout the study period. The correlation between UHI intensity and NDBI was positive. The findings of this study can help us better understand the dynamics and driving mechanisms of the urban heat environment. Furthermore, they can assist urban metropolitan planners in developing more efficient mitigation strategies that reduce the negative impacts of UHI and PM_{2.5} concentrations on the environment.

Keywords: Surface Urban Heat Island (SUHI); land surface temperature (LST); PM_{2.5}; Normalized Difference Building Index (NDBI)



Citation: El Afandi, G.; Ismael, H. Spatiotemporal Variation of Summertime Urban Heat Island (UHI) and Its Correlation with Particulate Matter (PM_{2.5}) over Metropolitan Cities in Alabama. *Geographies* **2023**, *3*, 622–653. <https://doi.org/10.3390/geographies3040033>

Academic Editor: Elzbieta Bielecka

Received: 27 August 2023

Revised: 28 September 2023

Accepted: 30 September 2023

Published: 2 October 2023



Copyright: © 2023 by the authors. Licensee MDPI, Basel, Switzerland. This article is an open access article distributed under the terms and conditions of the Creative Commons Attribution (CC BY) license (<https://creativecommons.org/licenses/by/4.0/>).

1. Introduction

According to the World Bank's global development data, of the projected growth of the world's urban population between 2018 and 2050, the global urban population is expected to double by 2050, with 56% of the world's population, or 4.4 billion, living in cities, and by then, 7 out of 10 people will reside in cities [1]. Therefore, urbanization is growing increasingly, causing an increase in air pollutants and urban heat islands (UHIs) [2–5]. Particularly, these changes to the Earth's natural landscape are highly visible and linked to two major challenges: population growth and climate change [6,7]. It significantly changes urban land use and air pollutant emissions, causing several environmental problems [8,9]. As a result, the thermal properties of the land surface change with the land use/land cover (LULC) structure in cities, which exacerbates the intensity of surface UHI [10]. According to relevant studies, this, in turn, worsens air quality and

increases pollutant concentrations [11–15]. In addition, there is evidence that UHI and air pollution are closely interlinked, and UHI-affected areas are more likely to experience air pollution [16]. It can lead to a rise in temperatures, which can in turn worsen the photochemical reaction that produces secondary pollutants [17]. Moreover, anthropogenic heat discharge from various sources such as transportation, industry, and human activities are directly related to UHI and may affect the spatiotemporal dynamics of the PM_{2.5} concentrations [18–20]. A significant proportion of air pollutants consists of PM_{2.5}, which can potentially increase the risk of cerebrovascular and respiratory diseases, posing a threat to human health [21,22]. Therefore, it is crucial to address air pollution and the Urban Heat Island (UHI) effect carefully. The combination of heat and pollution can lead to increased exposure to hazards [23,24].

The urban heat island (UHI) phenomenon refers to higher temperatures in cities compared to rural areas, creating the impression of a hotter island within the urban landscape [25]. Studies indicate that urban heat island (UHI) formation is caused by anthropogenic overheating from activities such as transportation, industry, and human behavior, along with CO₂ and pollution emissions. For example, some studies highlighted the impact of greenhouse gas emissions on UHI [23,26]. Others have shown that high levels of pollutants can cause excess heat islands and affect vertical temperature, potentially impacting the dispersion of particulate matter [27,28]. The difference in temperature between urban and rural areas, also known as the $T_{\text{urban-rural}}$ effect, is a direct result of this phenomenon [29,30].

Most of the research conducted in this field has primarily centered on the major metropolitan cities. It indicated that Urban Heat Islands (UHIs) tend to be stronger during the summer months, including heat waves [20,24,27,31–39]. These findings emphasize the criticality of addressing UHI and taking urgent action to mitigate its impact on human health and the natural environment. Thus, it is worth noting that the impact of urbanization on the size and intensity of UHI cannot be overlooked. The earliest recorded microclimatic phenomenon was documented by Howard in 1833 in the City of London. Other major cities, including New York [40], Moscow [41], and Beijing [10], as well as smaller cities like Eilat [42] and Tonami in Japan [24,43], have also experienced this phenomenon.

A lot of research has been done on how UHI varies in space and time. It found that these variations are affected by factors like weather conditions, land use, and the diversity of land cover [19,44–50]. A research study conducted in 65 cities across North America discovered a positive connection between urban heat island (UHI), precipitation, and population logarithm. The study specifically focused on Los Angeles, where the correlation was observed to be significant [51]. In addition, other studies have confirmed a direct linear relationship between temperature and air pollution in Atlanta over nine years [52,53]. The study provided detailed descriptions of urban heat islands in Atlanta and summertime convective thunderstorms [52]. The effects of land use and land cover (LULC) transformation on UHI, pollution, and health were also investigated in Atlanta between 1973 and 1998 due to the city's population doubling during this time [54]. Other cities that experienced similar incidents include Sacramento, San Francisco, Fresno, Houston, and Oklahoma. Lastly, it was reported that PM_{2.5} formations corresponded with changes in emission levels of smoke, NO_x, and biogenic volatile organic compounds (VOCs) [55].

In 2014, research conducted by Ying and Zhang showed that fine particles known as PM_{2.5} could reduce the intensity of the urban heat island (UHI) during daytime hours [56,57]. Another study by Kim and Baik compared the climates of the six largest cities in South Korea [58], while Khorrami researched the time variation of Istanbul City [59]. Additionally, several studies analyzed the intensity of heat islands in metropolis cities (419 cities) using a comparative approach [60–62]. These studies were the most comprehensive urban climate studies to date. Le et al. and Meng et al. conducted a study on the urban impact on climate in 32 major cities in China [63,64]. All these studies used land cover data associated with remotely sensed surface skin temperature, which allowed for the accurate determination of the physical extent of urban regions and the extraction of temperatures within cities and their rural surroundings.

Previous studies have shown that there is a significant gap in our knowledge regarding the relationship between urban heat islands (UHI) and particulate matter (PM_{2.5}), which varies across different regions. Alabama is currently facing a greater risk from extreme heat events compared to other states in the USA [65].

The top three populous cities in Alabama, namely Birmingham, Montgomery, and Mobile, are facing significant challenges related to UHI and air pollution due to their established economies, high population densities, and industrial employment. To address these challenges, this study aims to investigate the spatiotemporal variation of UHI and its correlation with PM_{2.5} concentrations in these cities over three years, 2002, 2012, and 2022. The results of this study will help government planning offices develop effective policies to reduce UHI and improve air quality.

The study has the following objectives: (a) to determine land use and land cover changes, land surface temperature variations, and their effect on UHI in the three urban cities during 2002, 2012, and 2022; (b) to determine the spatiotemporal variations of normalized difference built-up index (NDBI) and PM_{2.5} concentrations in the three cities; (c) to apply a spatial interpolation model to estimate PM_{2.5} concentrations in the three cities.

2. Data and Methodology

2.1. Description of the Study Area

This study will be conducted on the urban heat island (UHI) and PM_{2.5} concentration levels in three of Alabama's most highly populated cities, which have not been studied before. These cities, listed from north to south, are Birmingham, Montgomery, and Mobile, as depicted in Figure 1.

Here's a brief overview of each City's general characteristics:

Birmingham, the third most populated city in Alabama after Huntsville and Montgomery, is located between 33°31'14" and 33°52'06" N latitude, 86°48'09" and 86°80'24" W longitude. As of the 2021 census estimates, its population is 197,575, which is a 1% decrease from 2020. In 2021, the greater Birmingham metropolitan region had a total population of 1,115,289, making it Alabama's largest metropolitan area and the 50th most populous in the country. Due to its size, it can be effectively compared to a mid-sized City like Shelby, which is a nearby rural area.

Montgomery, the county seat of Montgomery County and the state capital of Alabama is located between 32°22'20" and 32°36'08" N latitude 86°17'09" and 86°30'22" W longitude. According to the 2021 census, it has a population of 200,603 people. The Montgomery metropolitan statistical area had a population of 386,047 in 2021, ranking it fourth in the state and 142nd in the United States. It can be effectively compared to a mid-sized City like Pick, which is in a nearby rural area.

Mobile is a city in the southwestern corner of Alabama, located between 30°41'40" and 30°43'59" N, 87° N latitude, 87°43'13"–88°02'35" W longitude. The City's area is approximately 180.06 sq. mi (466.34 km²), with land covering about 39.47 sq. mi (361.22 km²) and water covering about 40.59 sq. mi (105.12 km²) according to the US Gazetteer files in 2022.

2.2. Data

2.2.1. Land Surface Temperature (LST) Data

The production of LULC, calculation of LST, and extraction of the NDBI index will be based on satellite images obtained by Landsat 7 ETM and Landsat 8 OLI/TIRS during the summers of 2002, 2012, and 2022 as shown in Table 1. These images have a reasonable spatial resolution of 30 m for reflectance and 100 m for tropical bands. The cloud cover for all imagery is minimal, at only 10%, and the image quality is high, ranking 9. Preprocessing of level-1T scenes involved stacking, sub-setting the three cities, and removing cloud-contaminated pixels. The OLI band digital numbers (DN_s) were then radiometrically

calibrated by converting DN_s into at-sensor spectral radiance ($w/m^2/sr/nm$) and top-of-atmosphere (TOA) reflectance, corrected for solar elevation angle [66].

$$TOA\ p\lambda = \frac{ML * Qcal + AL}{\sin(\theta)}$$

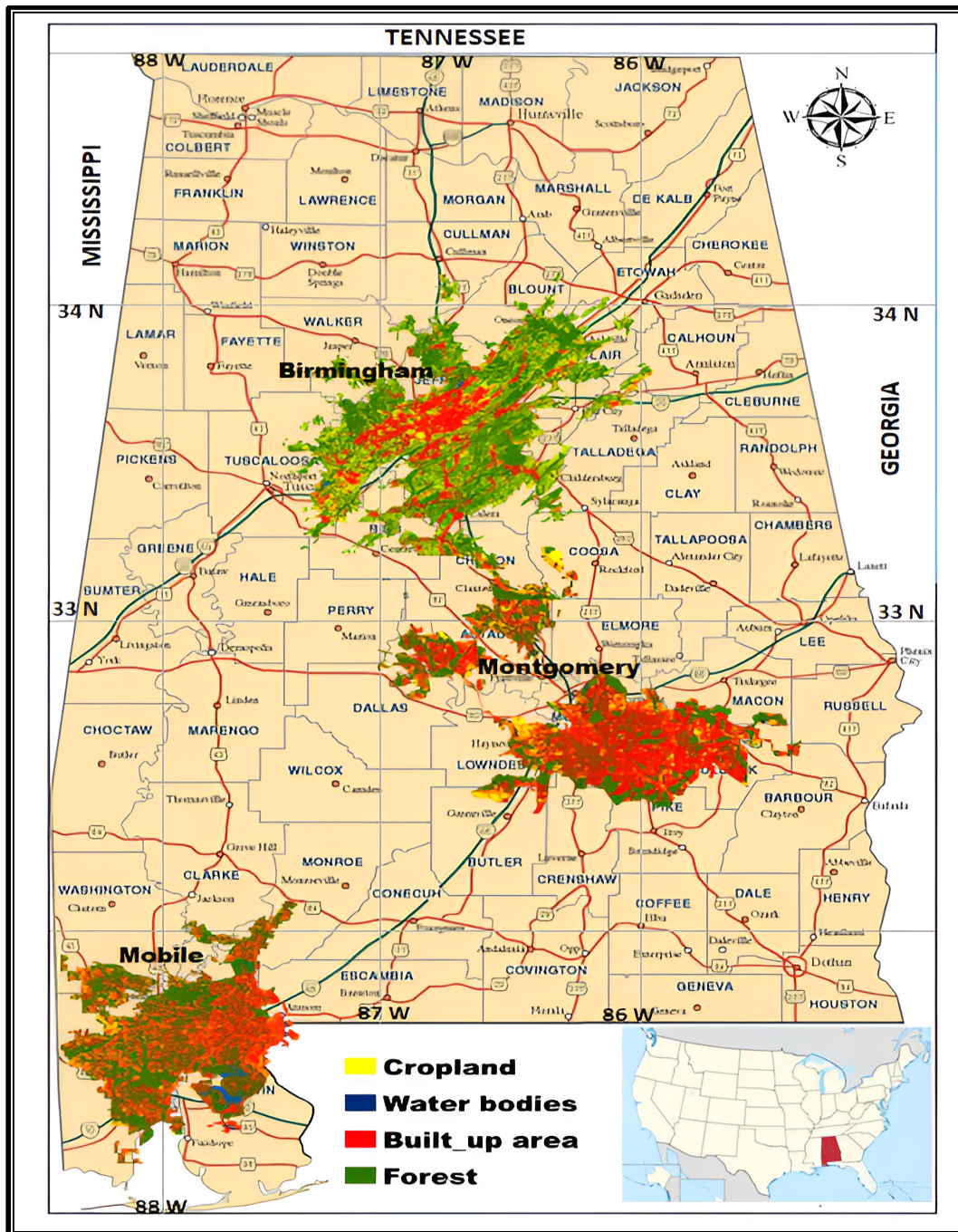


Figure 1. The study area.

The formula for $p\lambda$ involves TOA planetary reflectance, which hasn't been corrected for solar angle, and $Qcal$, which refers to OLI DN_s. Additionally, the ML and AL scaling factors for bands 1–7 are included in the metadata file, as is the solar elevation angle (θ). To achieve accurate results, an essential atmospheric correction was performed using the “Dark Object Subtract” image-based technique to calculate at-surface reflectance. The

spatial resolution of the OLI bands was enhanced to 15 m by utilizing the 15-m resolution panchromatic band and the “Principal Component” technique [66].

Table 1. Details of the Landsat images used in the study.

Sensor	Path/Raw	Location	Acquisition Date	Time (GMT)	K1	K2	Resolution (PAN/MS/TIRS)
Landsat 7 ETM+	020/037	32.29 N–86.40 W	7 July 2002	18:26:00	607.56	1260.56	15/30/60 m
	021/038	33.17 N–86.78 W					
	021/039	30.54 N–87.87 W					
Landsat 8 OLI/TIRS	020/037	32.29 N–86.40 W	7 August 2012	18:45:03	774.88	1321.07	15/30/100 m
	021/038	33.17 N–86.78 W					
	021/039	30.54 N–87.87 W					
Landsat 8 OLI/TIRS	020/037	32.29 N–86.40 W	7 July 2022	18:59:17	774.88	1321.07	15/30/100 m
	021/038	33.17 N–86.78 W					
	021/039	30.54 N–87.87 W					

2.2.2. Fine Particulate Matter (PM2.5) Data

From 2002 to 2022, the severity of air pollution in three cities was significant. Therefore, it was necessary to study the evolution of PM2.5 concentrations during this time. To achieve this, the study utilized data obtained from the US Environmental Protection Agency (EPA) (<https://www.epa.gov/outdoor-air-quality-data/download-daily-data>) (accessed on 21 July 2023) on daily PM2.5 concentrations from 24 air quality sites in metropolitan cities in Alabama during summertime. Although the study was limited to a few stations, it investigated the spatial distribution of PM2.5. The study calculated the daily PM2.5 concentration in each city by averaging data from different sites in the years 2002, 2012, and 2022.

2.3. Methods

To achieve the goals of the study, various techniques will be utilized. Firstly, NDVI and NDBI will be extracted to investigate the variations in LST and LULC types. Secondly, Landsat 8 TIRS thermal band images and Landsat 7 ETM+ will be used to calculate LST. Thirdly, a study of the urban-rural gradient will be conducted to compare the spatiotemporal variation of UHI and NDBI. It is important to classify Birmingham, Montgomery, and Mobile as LULC, which summarizes all UHI forcing variables. A parametric supervised classification using the maximum likelihood algorithm on the OLI scene will be used to distinguish between the key land covers of the cities and surrounding areas, such as cropland, forest, built-up areas, and water bodies. The accuracy of the classification output will be assessed using overall classification accuracy. Images with a 30-m spatial resolution from Landsat 7 ETM+ and Landsat 8 will be used. Additionally, NDBI statistical analysis using LST will be conducted to examine the variation in the UHI pattern. ERDAS IMAGINE 2020 and ArcGIS 10.8.1 will be utilized to complete the methods. The following sections will provide a detailed explanation of the study’s methods.

2.3.1. LULC Classification Technique

This study will use a K-means clustering-based supervised classification technique and the maximum likelihood classifier to map land use and land cover (LULC) in the three cities. The Landsat dataset’s composite optical bands (bands 2, 3, and 4 in Landsat 7 and bands 3, 4, and 5 in Landsat 8) will be utilized for the LULC classification. The study will identify four LULC classes in the three cities, which include built-up areas, forests, agriculture, and water bodies. To validate the accuracy of the classified maps and assess the effectiveness of the classifier used, a classification accuracy assessment will be conducted.

2.3.2. Images Preprocessing

To enhance their accuracy and achieve superior outcomes, the Landsat 7 ETM+ and Landsat 8 TIRS thermal band images underwent geometrical and radiometric correction.

Before analyzing the images, several image processing techniques were employed, such as layer stacking, image sub-setting, atmospheric correction, and image resampling. The Landsat thermal bands were resampled to a spatial resolution of 30 m using the nearest neighbor approach.

2.3.3. UHI Calculation

To determine the LST, the study utilized Landsat 7 (ETM+) for the year 2002 and Landsat 8 (TIRS) for 2012 and 2022, which were obtained through the USGS Earth Explorer. For each of the three identified locations during the season, bands 6 (2002) and 10 (2012 and 2022) were used to estimate the brightness temperature, while bands 3 and 4 were used to calculate the NDVI (Normalized Difference Vegetation Index) and bands 4 and 5 were used to analyze the NDBI (Normalized Difference Building Index). The satellite data products were geometrically corrected. Therefore, the first step of the proposed work is to convert the DN_s of band 6 (2002) and band 10 (2012 and 2022) to at-sensor spectral radiance, which can be found in the metadata file of the satellite images by using a raster calculator tool. Additionally, several equations used in this study are provided in Appendix A.

2.3.4. NDBI Calculation

The index used to extract built-up features is known as the Normalized Difference Built-up Index (NDBI) and it can range from -1 to 1 . This index is commonly used as an indicator of urbanization and is calculated by downloading metadata files and images. The calculation of Band 4 and Band 5 plays a key role in determining this index. In the current study, the NDBI was utilized, which can be calculated by analyzing the relationship between the Red, near-infrared (NIR), and shortwave-infrared (SWIR) spectral channels as follows:

$$\text{NDBI} = \frac{\text{SWIR} - \text{NIR}}{\text{SWIR} + \text{NIR}}$$

2.3.5. PM2.5 Spatial Interpolation Model

Due to the uneven distribution of EPA sites in Birmingham, Montgomery, and Mobile, there is a significant spatial dependence of PM_{2.5} concentrations in these Alabama metropolitan areas. To fill in the missing values, a spatial interpolation algorithm will be utilized, with Kriging interpolation being a widely accepted method. The interpolation results have shown no bias and minimal variance, with higher accuracy than that of remote sensing inversion data [67–71]. The main concept of Kriging spatial interpolation is to estimate the value of unknown sites from nearby data, providing precise modeling of the entire geographical distribution of PM_{2.5} concentrations in all cities under study. For this investigation, the Kriging spatial interpolation method will be implemented using ArcGIS 10.8.1 software. A semi-variogram model with 24 interpolation points will be created using PM_{2.5} hourly average concentration data from the three metropolitan cities in Alabama during the summer of 2002, 2012, and 2022. Finally, a spatiotemporal PM_{2.5} map with visualization will be produced.

3. Results

3.1. LULC Changes

In this study, the Kappa coefficient was used to evaluate the accuracy of the LULC maps. Six hundred points were randomly selected from both the classified maps and the field/Google Earth in the same locations. The Kappa coefficient results indicate that the overall accuracy for each classified map was above 92.3% as shown in Table 2.

Figures 2–4 display maps that illustrate the classification of land use and land cover in Birmingham, Montgomery, and Mobile cities. These maps indicate a consistent increase in the built-up area from 2002 to 2022, a trend that is common in metropolitan areas as the population grows. Initially, the highest concentration of built-up areas was observed in the city centers in 2002, but it gradually spread to the suburbs in the following years. As a result, there has been a significant reduction in forest and cropland areas.

This study has found a notable trend in the evolution of land use and cover (LULC) where forests are being converted into croplands, which are then developed into built-up areas. This has been observed across Birmingham, Montgomery, and Mobile cities, with densification occurring particularly in the north and southwest urban agricultural interface areas of Birmingham. Interestingly, built-up areas have also increased in the urban agricultural interface areas of the three cities, while forests in the east-central and north-central suburban areas of the three cities have experienced a significant decline from 2002 to 2022.

Table 2. Kappa coefficient accuracy assessment of LULC maps.

Year	User's Accuracy (%)	Producer's Accuracy (%)	Overall Accuracy (%)	Kappa Coefficient (%)
2002	96.6	92.3	92.3	0.93
2012	95.4	89.4	93.5	0.95
2022	94.8	88.0	92.80	0.90

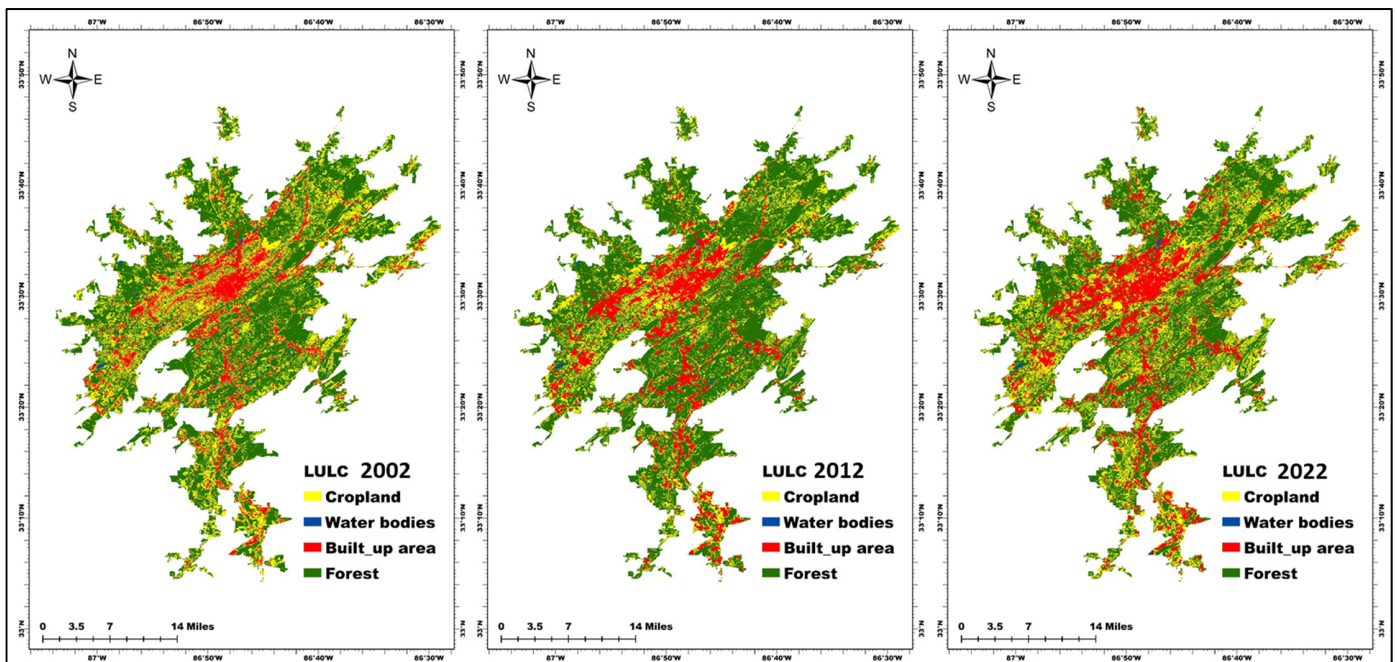


Figure 2. LULC changes in Birmingham during 2002, 2012, and 2022.

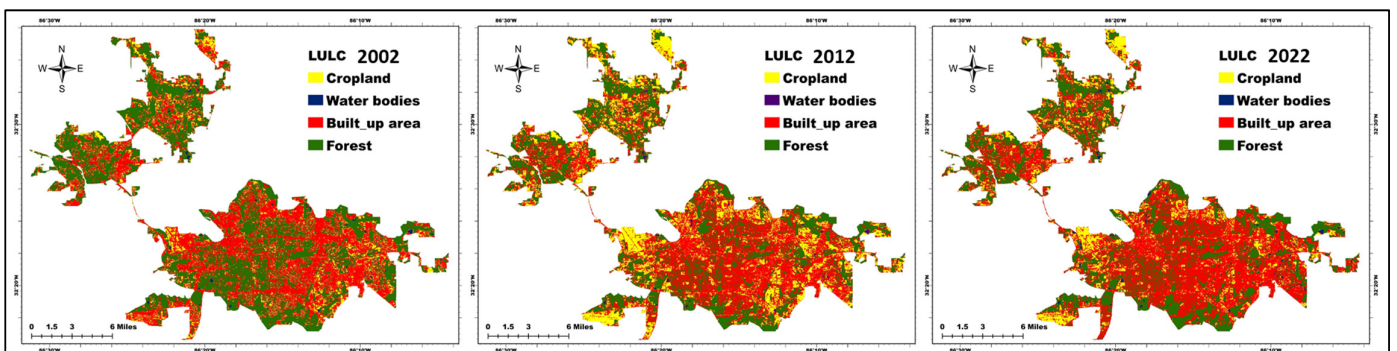


Figure 3. LULC change in Montgomery during 2002, 2012, and 2022.

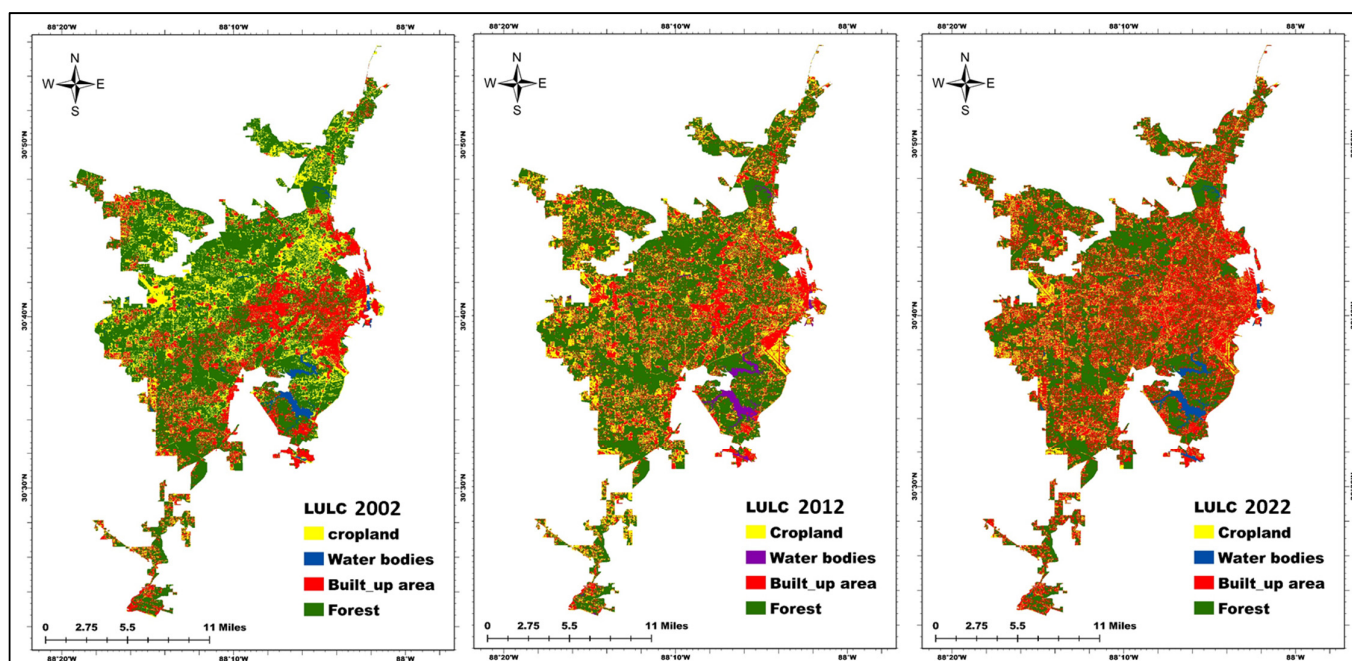


Figure 4. LULC change in Mobile during 2002, 2012, and 2022.

Table 3 provides statistical data on LULC changes in the three cities from 2002 to 2022. It shows a significant increase in built-up areas in Birmingham from 217.60 sq. km to 294.50 sq. km, in Montgomery from 170.48 sq. km to 205.57 sq. km, and in Mobile from 184.06 sq. km to 285.13 sq. km. However, croplands, forests, and water bodies have all shown a decline over the same period. In Mobile City, croplands have transformed into built-up areas in various parts except for the western areas. In Birmingham City, croplands have transformed into built-up areas in the north and west areas from 2002 to 2012, with other agricultural areas being added from 2012 to 2022. Meanwhile, the cropland area in Montgomery has experienced variation over the period from 2002 to 2022.

3.2. Spatiotemporal Variations of LST

Between 2002 and 2022, the LST in three cities has increased. Mobile had the highest LST, followed by Birmingham, with Montgomery having the lowest. In 2022, Montgomery had the lowest UHI compared to the other two cities. However, in 2012, Birmingham had a higher UHI than Montgomery and Mobile. A detailed study was conducted on the varying LST in Birmingham from 2002 to 2022, with temperature ranges of 19.30–34.20 °C in 2002, 20.50–36.70 °C in 2012, and 23.10–38.50 °C in 2022 as shown in Figure 5. The analysis of LST maps for this period shows a progressive pattern of high LST distribution. Patches of high LST were observed in downtown and northwestern suburban areas of Birmingham in 2002. By 2012, the patches of higher LST had increased in the northern and western urban-rural interface but declined in the northeastern suburban areas. The most significant change was noted in Birmingham downtown, where higher LST accumulation increased significantly in the central district while decreasing in the suburbs, especially in the north and east-west districts. In 2022, patches of higher LST increased in the eastern, northwestern, and southern parts of Birmingham, particularly in Jefferson, Springville, and Castle suburban areas, due to the expansion of built-up areas. Overall, the LST has increased in all Birmingham suburban areas from 2002 to 2022, with a minimum LST below 22 °C in all suburban areas in 2002 and increasing to over 28 °C in 2022 in most of Birmingham and its surroundings. The maximum LST was 32.70 °C in all rural areas, increasing to over 38.20 °C in most urban-rural interface areas in 2022, with the highest increase noted in eastern rural areas and central parts. Mean LST increased uniformly and significantly in Birmingham and surrounding areas during 2002–2022.

Table 3. LULC changes in Birmingham, Montgomery, and Mobile during (2002, 2012, and 2022).

Birmingham LULC Class	2002		2012		2022	
	Area in sq. km	Area in %	Area in sq. km	Area in %	Area in sq. km	Area in %
Built-up area	217.60	13.10	242.00	14.56	294.50	17.73
Cropland	478.60	28.80	367.25	22.10	465.81	28.03
Forest	957.18	57.61	1042.63	62.75	891.88	53.70
Water bodies	8.05	0.48	9.53	0.57	9.22	0.55
Total	1,661,410	100	1,661,410	100	1,661,410	100

Montgomery LULC Class	2002		2012		2022	
	Area in sq. km	Area in %	Area in sq. km	Area in %	Area in sq. km	Area in %
Built-up area	170.48	42.60	182.20	45.53	205.57	51.37
Cropland	47.54	11.88	59.48	14.86	55.40	13.84
Forest	179.84	44.94	156.35	39.07	136.07	34.00
Water bodies	2.3292	0.58	2.169	0.54	3.164	0.79
Total	4,001,994	100	4,001,994	100	4,001,994	100

Mobile LULC Class	2002		2012		2022	
	Area in sq. km	Area in %	Area in sq. km	Area in %	Area in sq. km	Area in %
Built-up area	184.06	26.91	211.22	30.88	285.13	41.68
Cropland	130.26	19.04	120.78	17.66	90.97	13.30
Forest	359.20	52.51	342.21	50.02	295.47	43.19
Water bodies	10.59	1.55	9.8811	1.44	12.546	1.83
Total	684.1026	100	684.1026	100	684.1026	100

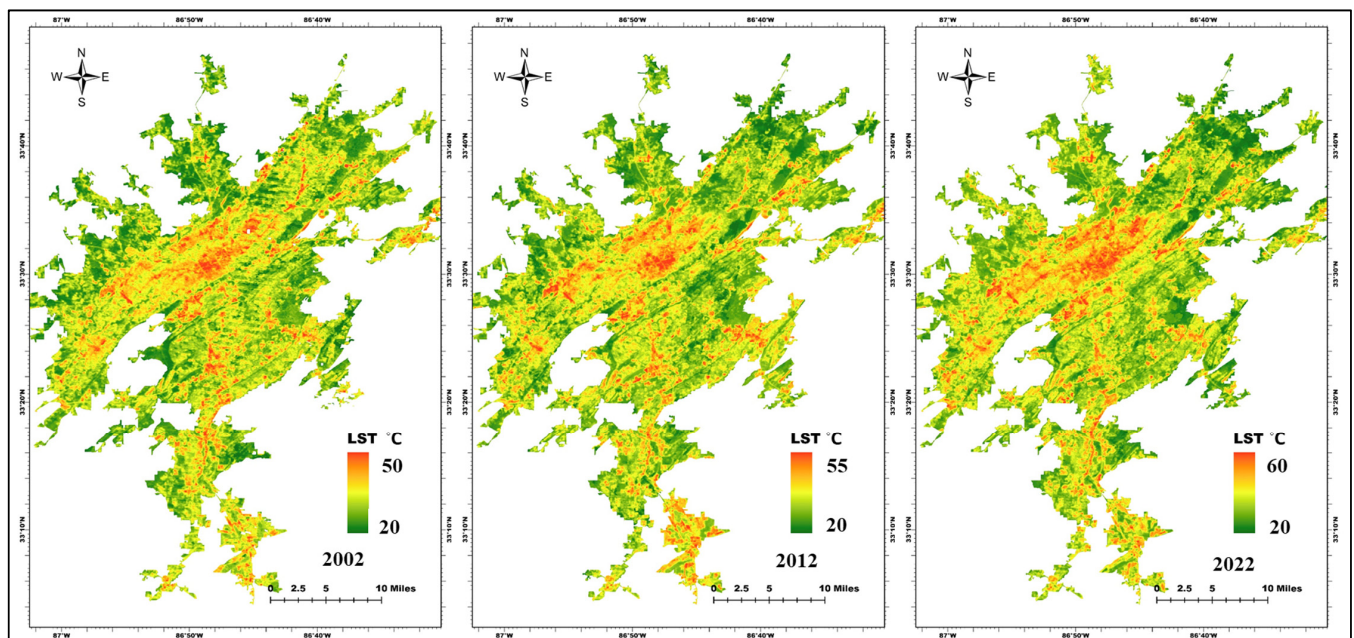


Figure 5. Spatiotemporal Variation of LST pattern in Birmingham during 2002, 2012, and 2022.

Based on the LST analysis shown in Figure 6, it is evident that the Land Surface Temperature (LST) in Montgomery varied from 22.40 °C to 36.20 °C in 2002, 22.90 °C to 38.30 °C in 2012, and 23.20 °C to 39.40 °C in 2022. The LST maps of Montgomery between 2002 and 2022 demonstrate that areas with high LST have gradually increased due to urban

expansion and economic growth. Montgomery's economy has diversified and grown in recent years, leading to regeneration projects along the Alabama River and infrastructure improvements along the Selma to Montgomery National Historic Trail.

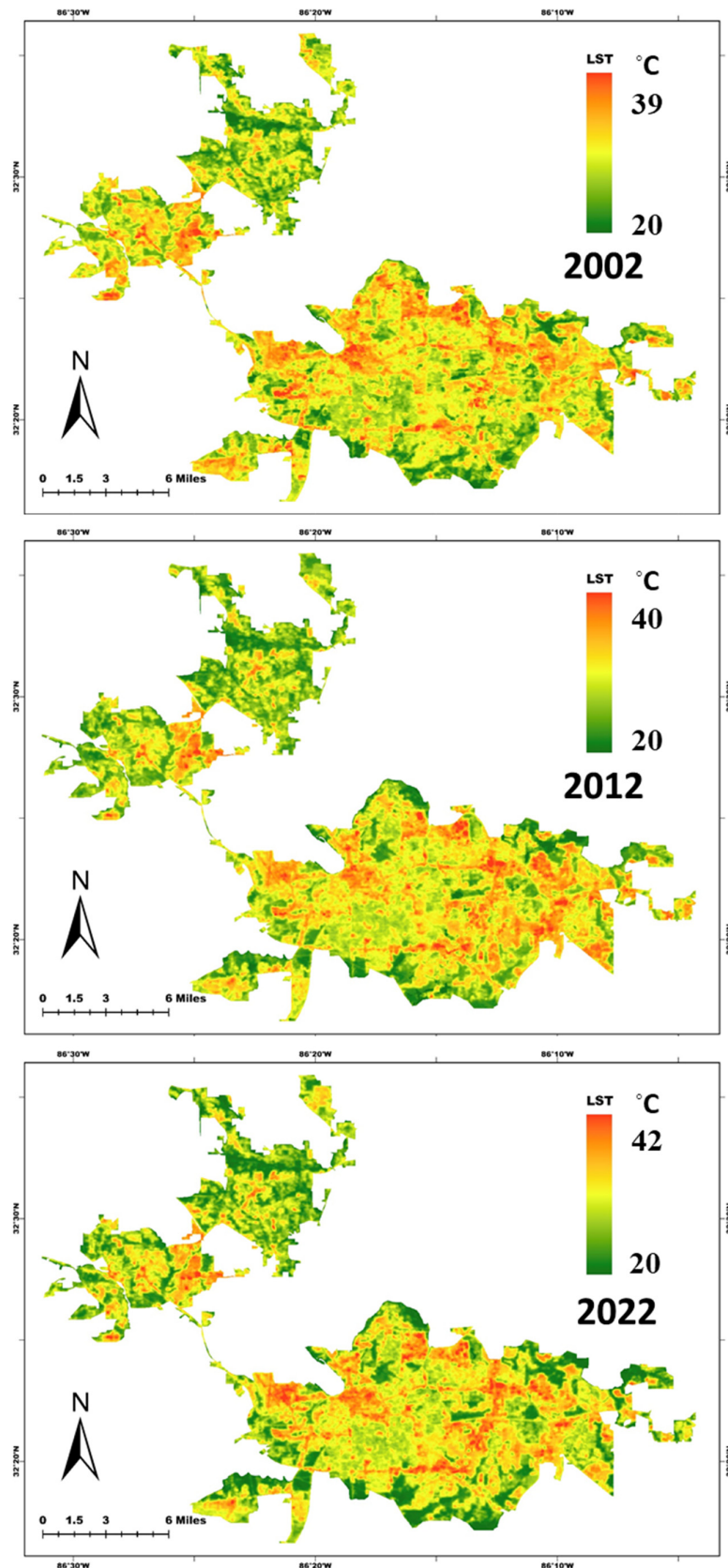


Figure 6. Spatiotemporal Variation of LST pattern in Montgomery during 2002, 2012, and 2022.

Between 2002 and 2022, Montgomery City experienced an increase in high LST patches, particularly in suburban areas such as Lapine, Mathews, Pike, Pine Level, and Ramer. This growth was due to economic development plans and the expansion of built-up areas. The downtown and east sides of the city saw the most growth, with new neighborhoods and big-box stores being developed. Conversely, LST was moderate in the southwestern suburban areas, and the rural boundaries of the city showed a reduction in LST. The suburban areas experienced the most significant change in LST patterns, with large increases noted. Overall, Montgomery's LST uniformly increased in all suburban areas during 2002–2022. In 2002, the minimum LST was below 23.20 °C in all suburban areas, but by 2022, it had increased to more than 29.30 °C in most of the city and its environs. Similarly, the maximum LST was 32.60 °C in all rural areas in 2002 and increased to more than 38.90 °C in most urban and rural interfaces in 2022, with the suburban areas of the downtown and eastern rural towns experiencing the highest increase. The mean LST also showed an extremely high but uniform increase in all of Montgomery and its surrounding areas during 2002–2022.

The results reported here indicate that Mobile City has undergone significant urban growth, encompassing 98% of the entire city and leading to widespread economic and commercial activity. Despite a 7% decrease in population between 2002 and 2022, Mobile's population increased to 204,689 individuals in the summer of 2022 after a successful vote to annex regions west of the municipal limits. This now makes it the second-most populated city in Alabama, after Huntsville (<https://www.al.com/news/2023/07/mobile-now-second-largest-city-in-alabama-after-annexation-vote.html>) (accessed on 1 August 2023). Figure 7 illustrates that the land surface temperature (LST) in Mobile ranged from 21.10 °C to 33.80 °C in 2002, 21.50 °C to 35.20 °C in 2012, and 23.00 °C to 37.60 °C in 2022, despite the aforementioned population decline.

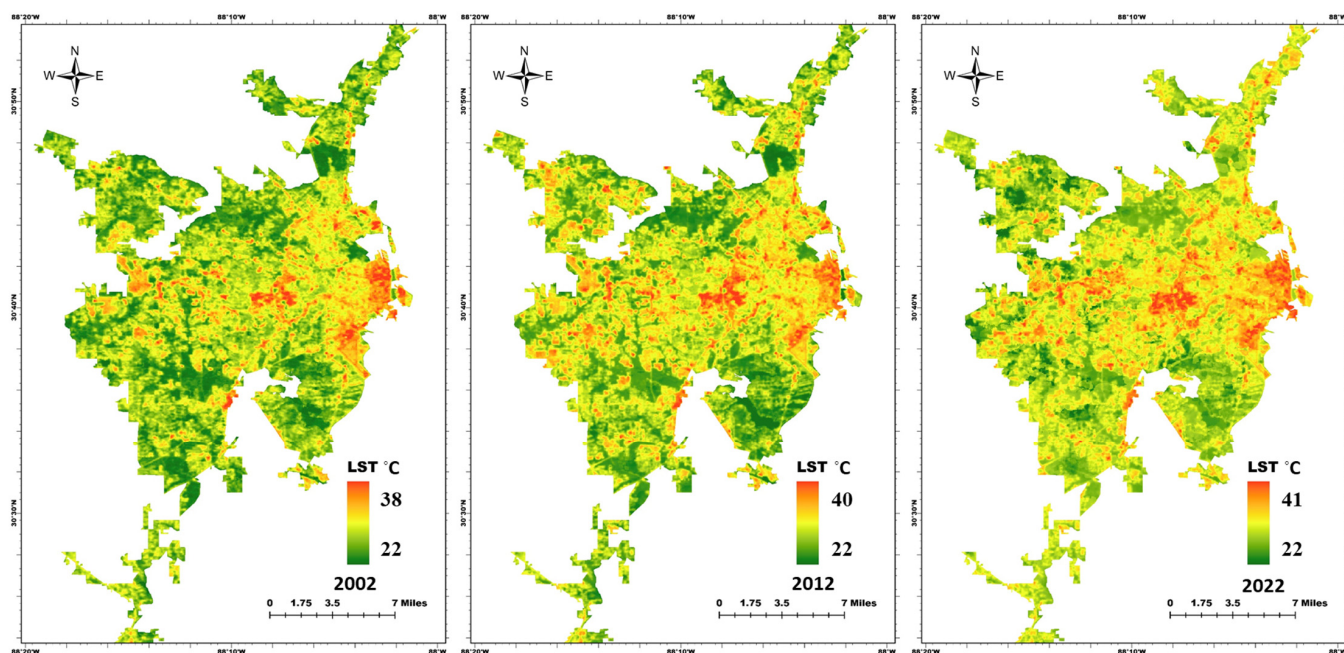


Figure 7. Spatiotemporal Variation of LST Pattern in Mobile during 2002, 2012, and 2022.

After analyzing Mobile's LST maps from 2002 to 2022, it was discovered that high LST levels were increasing due to human activities and global warming. In 2002, there were only a few patches of high LST around the Port of Mobile, with scattered patches in the west and south. LST was high in Prichard, Bucks, and Saraland, but moderate in Culfcrest, Baldwin, and Satsuma. However, by 2012, patches of higher LST had increased in the central, northern, and western parts of Mobile. The most significant LST increase occurred in downtown Mobile, where clusters of higher LST grew significantly in the south, including Tillmans Center, Grand Bay, and Belle Fontane, and the middle of Mobile City,

including Semmes, Satsuma, Chickasaw, and Theodore. The western suburban areas of the city, however, experienced a decline in LST. By 2022, patches of higher LST had increased in the middle, northwestern, and southern parts of the entire Mobile city, particularly in Tillmans, Prichard, Grand Bay, and Saraland. The growth of Mobile’s manufacturing and industrial sectors led to increased urban expansion and the rebuilding of service buildings in the city and its suburban areas, making it an attractive hub for businesses.

It was observed that thermal variation in Mobile showed that the LST increased in all suburban areas during 2002–2022. Additionally, the minimum LST was below 24 °C in all suburban areas in 2002 and increased to over 32 °C in 2022 in most of Mobile and its surroundings. Similarly, the maximum LST was 34.40 °C in all urban areas, increasing to more than 41.60 °C in most of the urban and rural interface in 2022. The central parts had the highest increase in maximum LST. Furthermore, the mean LST showed an extremely high but uniform increase in almost all of Mobile and its surrounding areas during 2002–2022.

3.3. Effects of LULC Change on UHI

Table 4 shows the average LST and temperature difference (°C) for the primary LULC class in Birmingham, Montgomery, and Mobile City, as well as their rural areas, in 2002, 2012, and 2022.

Table 4. The mean LST and its difference (°C) for the main LULC class in Birmingham, Montgomery, and Mobile Cities in 2002, 2012, and 2022.

Birmingham LULC Class	Mean LST			Mean LST Difference		
	2002	2012	2022	2002–2012	2012–2022	2002–2022
Built-up area	34.10	36.50	38.00	1.90	1.50	3.90
Cropland	33.20	33.30	33.60	0.10	0.30	0.40
Forest	31.00	31.50	31.80	0.50	0.70	0.20
Water bodies	23.30	23.10	23.30	0.20	0.80	1.00
Montgomery LULC Class	Mean LST			Mean LST Difference		
	2002	2012	2022	2002–2012	2012–2022	2002–2022
Built-up area	36.20	36.80	39.40	0.60	2.60	3.20
Cropland	26.50	25.40	26.00	−0.90	0.60	−0.50
Forest	23.00	23.10	23.00	0.10	−0.10	0.00
Water bodies	22.10	22.00	22.30	0.10	−0.10	−0.20
Mobile LULC Class	Mean LST			Mean LST Difference		
	2002	2012	2022	2002–2012	2012–2022	2002–2022
Built-up area	33.40	36.00	37.20	2.60	1.20	3.80
Cropland	28.40	28.50	28.10	0.10	−0.40	−0.30
Forest	24.20	24.00	23.60	0.20	−0.40	−0.40
Water bodies	23.00	23.50	23.60	0.50	0.10	0.30

Between 2002 and 2012, the average land surface temperature (LST) of built-up areas in Birmingham City increased from 34.10 °C to 36.50 °C, a difference of 1.90 °C. In 2022, the mean LST for built-up areas rose even higher to 38.00 °C, an increase of 1.50 °C from 2012. This trend was not observed in cropland, which had a mean LST of 33.20 °C in 2002, 0.10 °C lower than the mean LST in 2012, and 0.30 °C lower than in 2022. This could be because cropland is more exposed to solar radiation and bare soil during the summer. In contrast, forests had a mean LST of 31.00 °C in 2002, which increased to 31.50 °C in 2012 and 31.80 °C in 2022. A closer inspection at the data shows that the forest class had a 0.70 °C higher LST in 2012 compared to 2002 and 0.20 °C higher than in 2022. Water bodies

consistently had lower LSTs than other land use and land cover (LULC) classes, with mean LSTs of 23.30 °C, 23.10 °C, and 23.30 °C in 2002, 2012, and 2022, respectively.

In Montgomery City, the average land surface temperature (LST) for developed areas was 36.20 °C in 2002. By 2012, it had increased to 36.80 °C, which was 0.60 °C higher than in 2002. In 2022, the average LST for developed areas was 39.40 °C, which was 2.60 °C higher than in 2012 and 3.20 °C higher than in 2002. Cropland had an average LST of 33.50 °C in 2002, which was 0.90 °C lower than the average LST in 2012 and 0.50 °C lower than in 2022. Meanwhile, the forests had an average LST of 31.00 °C in 2002, which increased slightly to 31.10 °C in 2012 and then to 31.40 °C in 2022. The forest category experienced a 0.70 °C higher LST in 2012 compared to the average LST in 2002 and 0.40 °C higher than in 2022. Conversely, water bodies had lower LSTs compared to other land use and land cover (LULC) classes, with average LSTs of 24.10 °C, 24.00 °C, and 24.30 °C in 2002, 2012, and 2022, respectively.

The average land surface temperature (LST) for urban areas in Mobile City was 33.40 °C in 2002. By 2012, it had increased to 36.00 °C, which was 2.60 °C higher than in 2002. As predicted, the average LST for urban areas rose to 37.20 °C in 2022, which was 1.20 °C higher than in 2012 and 3.80 °C higher than in 2002. In comparison, cropland had an average LST of 28.40 °C in 2002, which was 0.10 °C higher than in 2012 and 0.40 °C lower than in 2022. Forests had an average LST of 29.20 °C in 2002, which increased to 30.00 °C in 2012 and then decreased to 28.00 °C in 2022. The forest area showed a 0.20 °C higher LST in 2022 compared to 2002 and was 0.40 °C lower than in 2012. Water bodies had lower LSTs than other land use and land cover (LULC) categories, with average LSTs of 25.00 °C, 25.50 °C, and 25.60 °C in 2002, 2012, and 2022, respectively.

3.4. Spatiotemporal Variations of NDBI

This study examines the index used to identify built-up features and urbanization indicators in three cities over multiple years, as shown in Figures 8–10. The NDBI values obtained range from -1 to 1 , indicating an increase in buildings and urbanization over time, with varying values. In all three areas surveyed, the number of buildings in 2022 exceeded those in 2012 and 2002. Moreover, Mobile has a higher number of buildings than Birmingham and Montgomery, making it the most populous city in Alabama due to its higher population density.

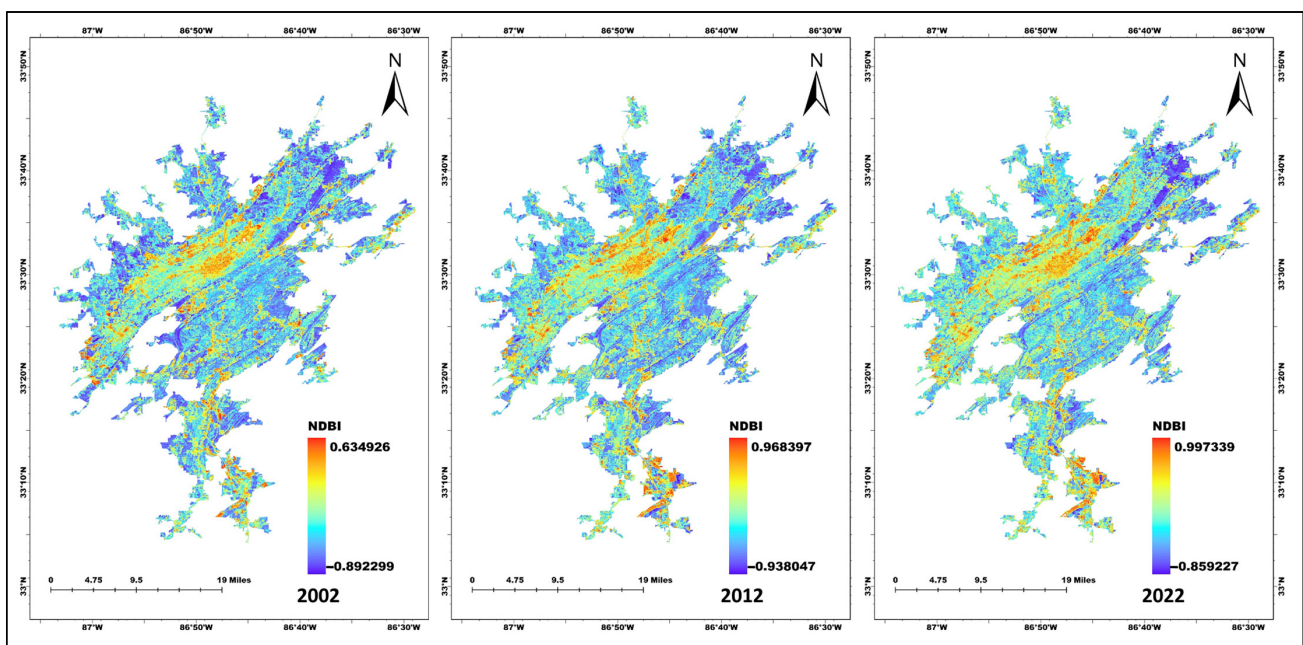


Figure 8. Spatiotemporal variations of NDBI in Birmingham City and its surroundings in 2002, 2012, and 2022.

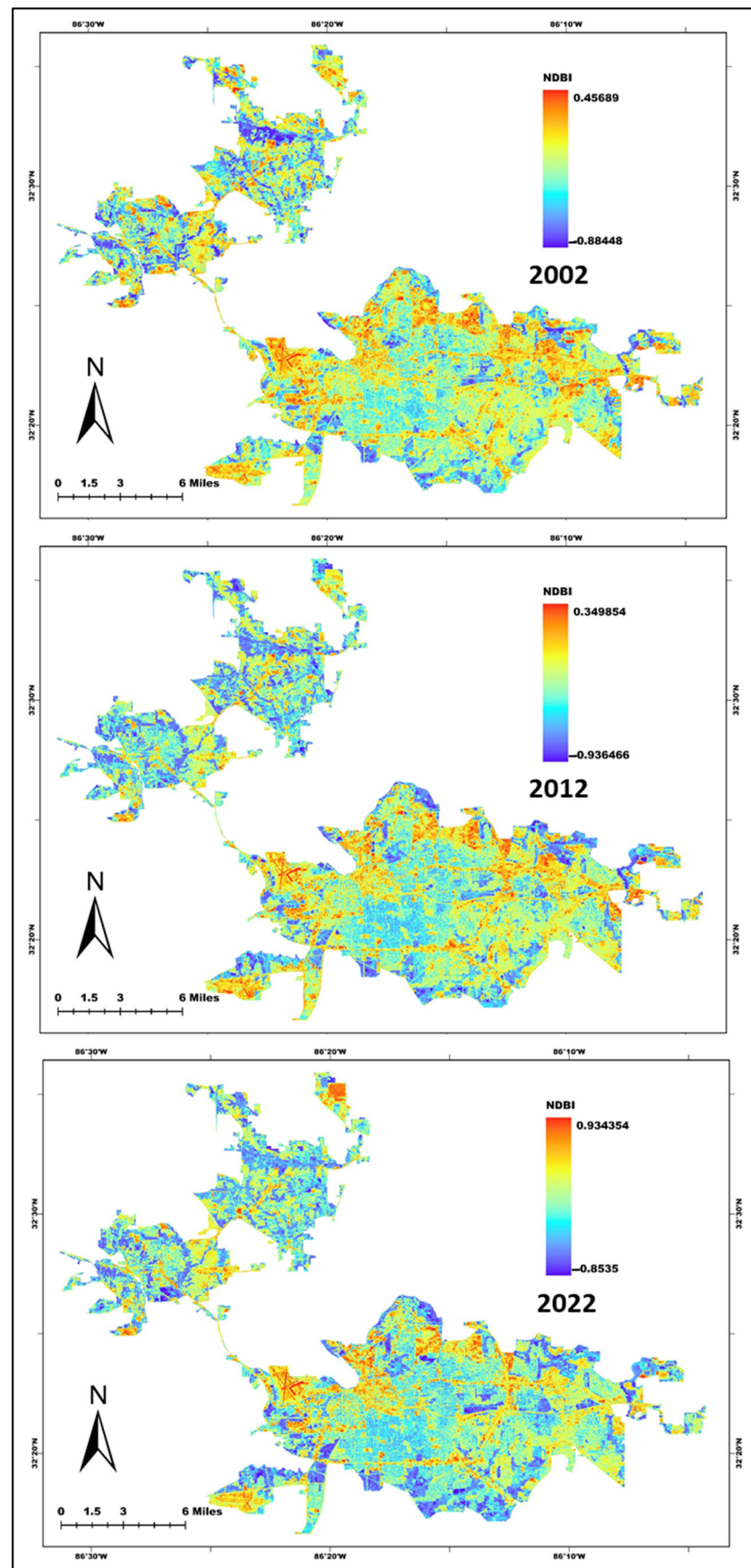


Figure 9. Spatiotemporal variations of NDBI in Montgomery City and its surroundings in 2002, 2012, and 2022.

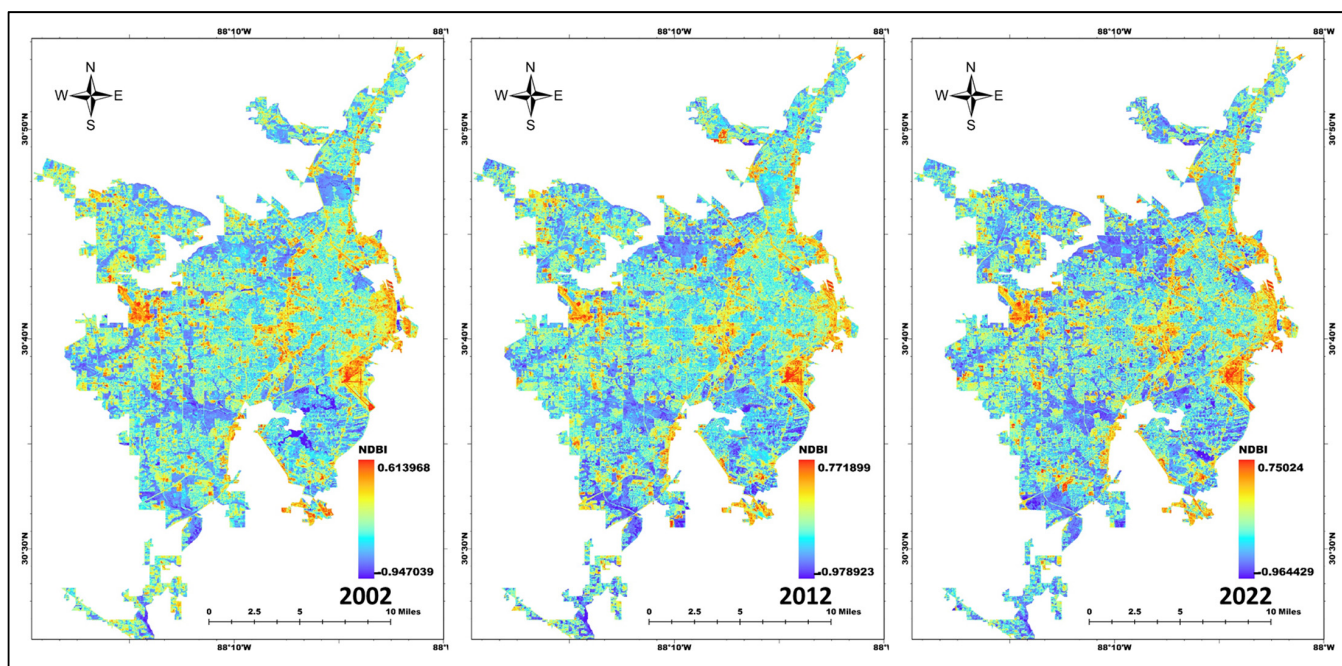


Figure 10. Spatiotemporal variations of NDBI in Mobile City and its surroundings in 2002, 2012, and 2022.

The image in Figure 8 displays how the Birmingham city urban area has grown towards the west, central, northwest, and south regions between 2002 and 2022. This expansion occurred due to the development of residential, industrial, urban, and other paved areas, which replaced forests, cropland, and uninhabited areas. The NDBI values in 2002 ranged from -0.89 to 0.63 , with an average of 0.76 . In 2012, the NDBI values ranged from -0.93 to 0.96 . By 2022, the maximum NDBI value reached 0.99 , while the minimum value was -0.85 . These results suggest that the urban regions' size and the amount of high-radiation urban materials have increased since 2002. Cropland had comparable NDBI values, meaning that NDBI and LST are positively correlated. In other words, lower NDBI values correspond to lower LST values, while higher NDBI values correspond to higher LST values.

From 2002 to 2022 (Figure 9), the urban area of Montgomery has expanded towards the east, central, northwest, and west parts. In 2002, the minimum and maximum NDBI values were -0.86 and 0.45 , respectively, with an average of 0.68 . In 2012, the minimum and maximum NDBI values were -0.93 and 0.35 , respectively. By 2022, the maximum NDBI value had increased to 0.93 , and the minimum had decreased to -0.85 . This suggests that the size of urban regions and the number of high-radiation urban buildings have increased since 2002. Like Birmingham, there is a positive correlation between NDBI and LST.

The expansion of Mobile City's urban area can be seen in Figure 10, with growth towards the east, central, northeast, and west regions from 2002 to 2022. The NDBI values in 2002 ranged from -0.94 to 0.61 , with an average of 0.75 . In 2012, the NDBI value ranged from -0.97 to 0.77 , and by 2022, the maximum NDBI value had decreased to -0.96 , while the minimum value remained at 0.75 . This suggests that urban regions have grown since 2002, and NDBI and LST are positively related. Figure 11 confirms a positive correlation between NDBI and UHI, with R^2 values of 0.46 , 0.41 , and 0.74 in 2002, 2012, and 2022, respectively. For more detailed data, please refer to Appendix B.

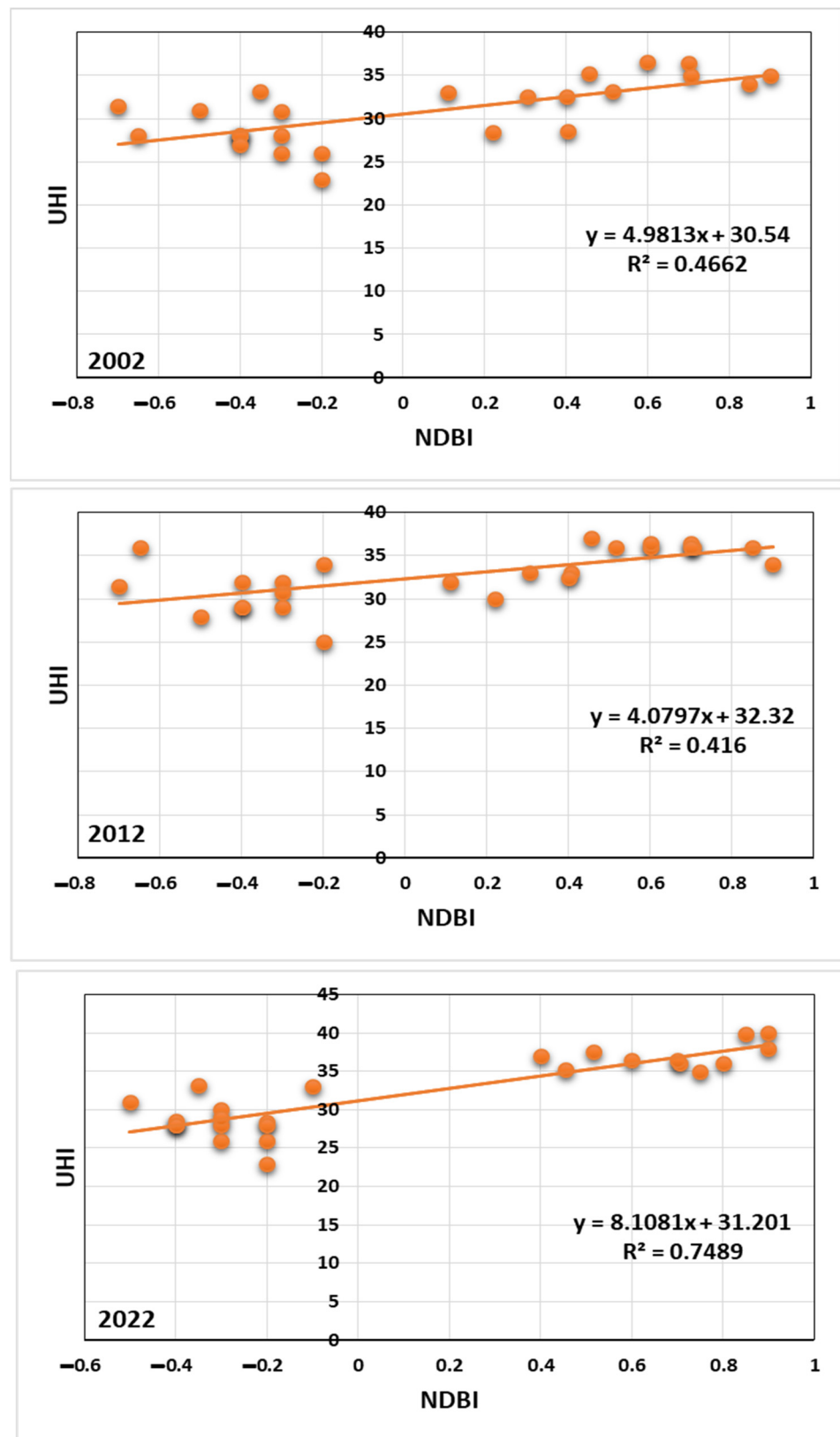


Figure 11. Scattered plots of UHI and NDBI of three cities in 2002, 2012, and 2022.

3.5. Spatiotemporal Variations of PM_{2.5} Concentration

The data presented in Figure 12 displays the PM_{2.5} concentrations measured in Birmingham, Montgomery, and Mobile City during the summers of 2002, 2012, and 2022.

Birmingham had the highest PM_{2.5} concentration, followed by Montgomery and Mobile. However, there was a significant decrease in PM_{2.5} concentrations in all three cities from 2002 to 2022, which was unexpected. Birmingham's PM_{2.5} concentration decreased by 50%, dropping from 34.2 in 2002 to 15.6 in 2012, and eventually to 7.1 $\mu\text{g}/\text{m}^3$ in 2022. Similarly, Montgomery's concentration decreased from 26.3 in 2002 to 14.1 in 2012, and eventually to 7.8 $\mu\text{g}/\text{m}^3$ in 2022. Mobile City also experienced a decrease from 18.1 in 2002 to 7.8 in 2012, and eventually to 4.4 $\mu\text{g}/\text{m}^3$ in 2022. The data also revealed that the PM_{2.5} concentrations at the urban-agricultural interface remained relatively constant in all three cities, while there was a gradual decrease in concentrations in the central and urban parts throughout the study period (2002–2022). This could be attributed to a combination of factors, including global warming and the heat island effect. Additionally, heavy summer rains aided in cleaning the air of pollutants, which significantly affected PM_{2.5} concentrations during the rise in temperature in these cities.

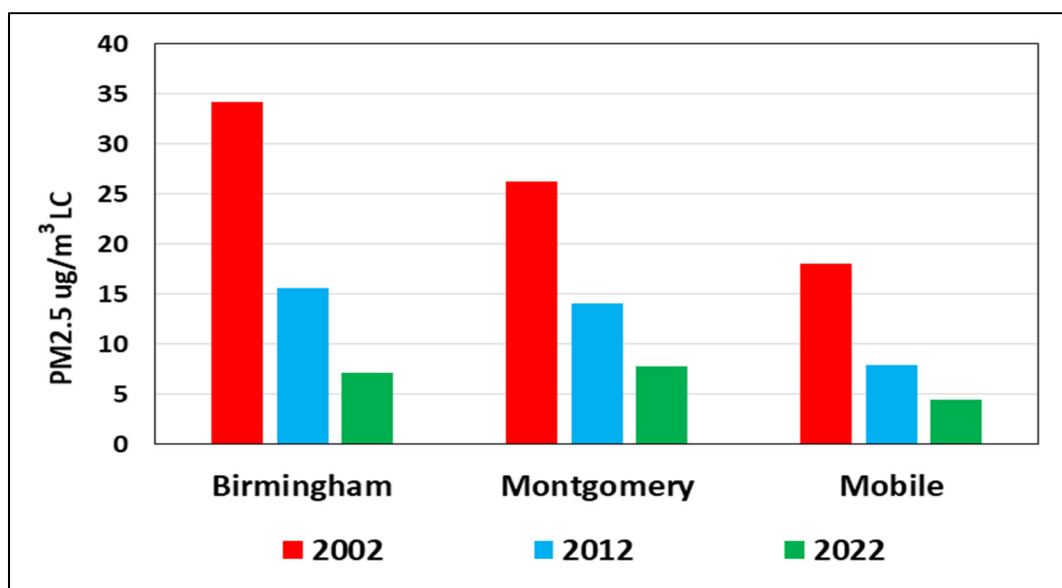


Figure 12. Particulate Matter (PM_{2.5}) concentration during 2002, 2012, and 2022 in summer.

3.6. PM_{2.5} Spatial Interpolation Model

It is worth noting that many studies have utilized interpolation techniques in computation to estimate PM_{2.5} concentrations when data is limited at certain stations. This enables them to effectively analyze PM_{2.5} concentration variation patterns [68,69,71–73]. For the years 2002, 2012, and 2022, a spatial interpolation method called Kriging was used to establish the geographic distribution of PM_{2.5} summer average concentrations. The Kriging method was used to determine summer average PM_{2.5} concentrations at ground stations and throughout the three cities, as shown in Figures 13–15.

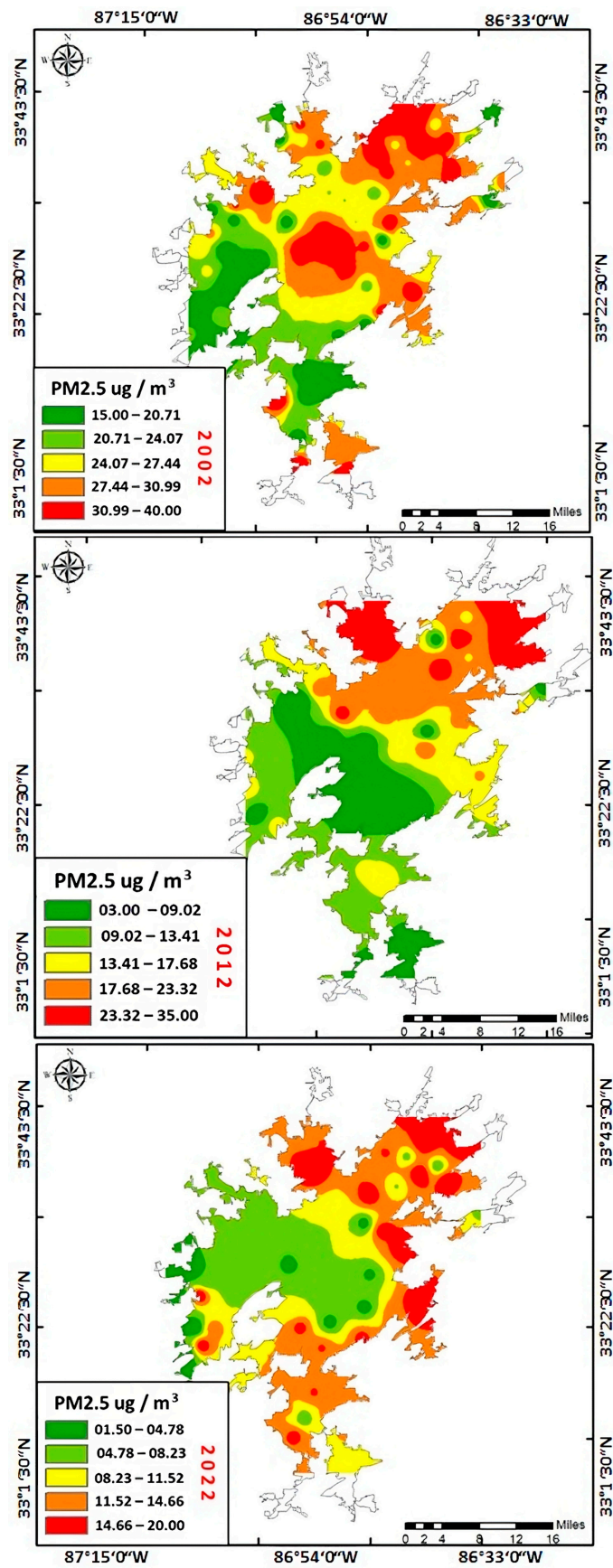


Figure 13. Spatial distribution of PM2.5 concentrations in Birmingham City during 2002, 2012, and 2022.

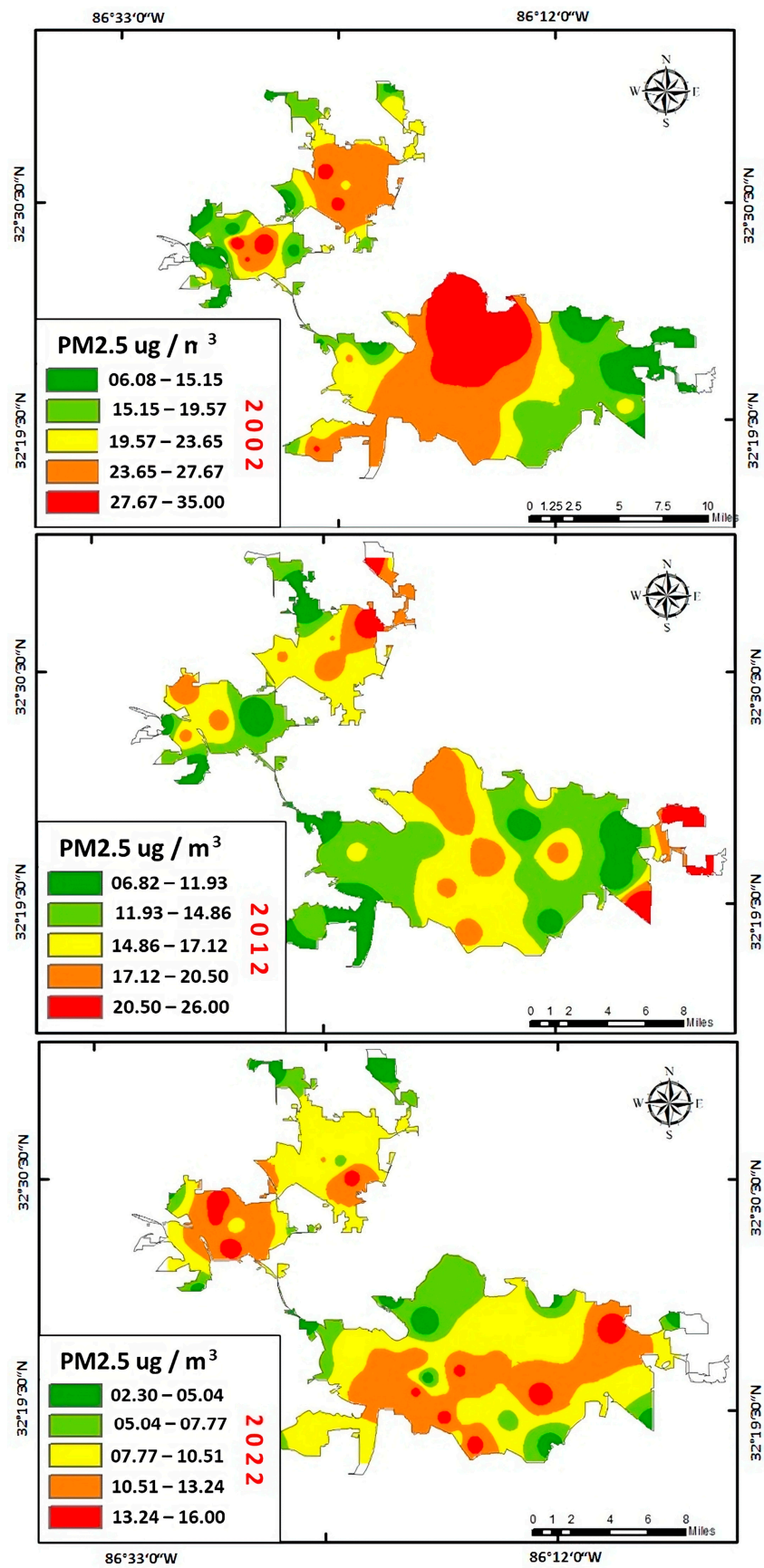


Figure 14. Spatial distribution of PM2.5 concentrations in Montgomery City during 2002, 2012, and 2022.

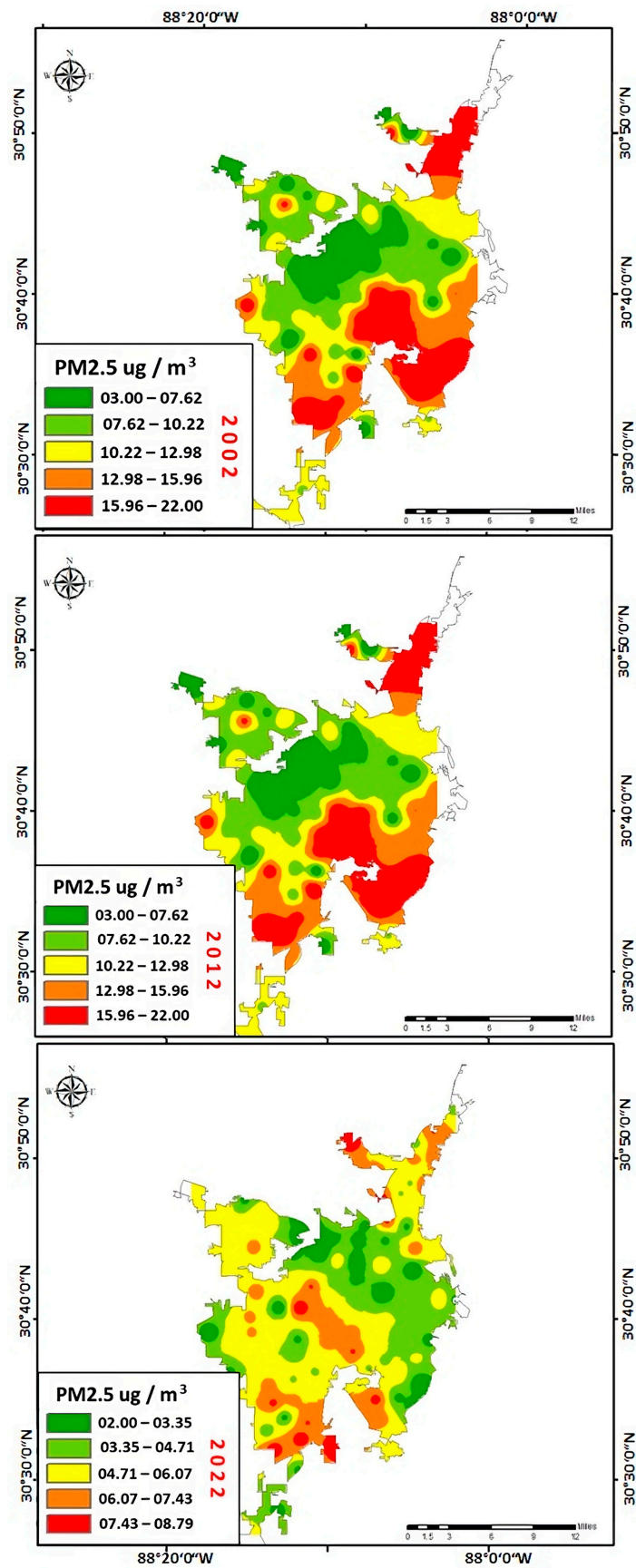


Figure 15. Spatial distribution of PM2.5 concentrations in Mobile City during 2002, 2012, and 2022.

Even though this method improved exposure coverage, the spatial resolution was not always adequate for predicting exposures at greater distances from monitoring stations. During the study period, PM_{2.5} concentrations decreased in most areas of the three cities, and the spatial pattern remained stable. Notably, a few primary clusters of regions with high PM_{2.5} concentrations were identified. As previously mentioned, the concentration of PM_{2.5} in densely populated areas was slightly higher than in suburbs, and the city downtown was not necessarily the source of pollution.

According to Figure 13, PM_{2.5} concentration in Birmingham was evenly spread across the city during the study period. The concentration decreased overall, but the distribution remained the same. Three clusters had the highest concentration of PM_{2.5}: the city center, northeast, and south. Notably, the north had the highest pollution levels in Hoover, Tarrant, Fultondale, and Watson, near Birmingham's downtown and airport intersection. From 2002 to 2012, PM_{2.5} concentration had a more significant impact on a larger area than in 2022. However, air quality has improved significantly between 2020 and 2022, with PM_{2.5}-induced pollution decreasing, as shown in Figure 13.

From 2002 to 2022, the average PM_{2.5} concentration in Montgomery City during the summer decreased year by year. The overall rate of decrease was 200%. Interestingly, the minimum rate of decrease occurred in 2012 (100.05%), while the highest rate of decrease occurred in 2022 (90.90%). Figure 14 shows that there was a distinct decrease pattern in Montgomery's PM_{2.5} concentration. Most of the city experienced a reduction in concentration during the study period, and the distribution remained steady. The two areas with the highest PM_{2.5} concentrations were downtown and the northeast of the city. Notably, the areas with the highest pollution levels were in the northeastern urban clusters, specifically in old Alabama town, Highland Ave, Mathews, Alabama State University, Remer, and Centennial Hill, close to the intersection of Montgomery's downtown and Pick Road. Between 2002 and 2012, the PM_{2.5} concentration in Montgomery was more severe across a wider area compared to 2022. However, there was a significant decrease in PM_{2.5}-induced pollution between 2002 and 2022, with the air quality improving in all US cities.

As expected, the analysis of the area found no notable difference in PM_{2.5} levels between Mobile, Birmingham, and Montgomery. However, Mobile experienced a significant reduction in PM_{2.5} levels, as illustrated in Figure 15. While most parts of Mobile City showed a decrease in PM_{2.5} concentrations, there were still four clusters of high levels located in Mobile downtown, the east, south, and southeastern parts of the city. The central urban regions of Mobile, including Airport, Rockery, Baltimore, Rosedale, and Maryville, exhibited particularly high levels of pollution, with most of them located near the downtown area. Additionally, Figure 16 indicates a significant negative correlation between LST and PM_{2.5} levels in Birmingham, Montgomery, and Mobile from 2002, 2012, and 2022.

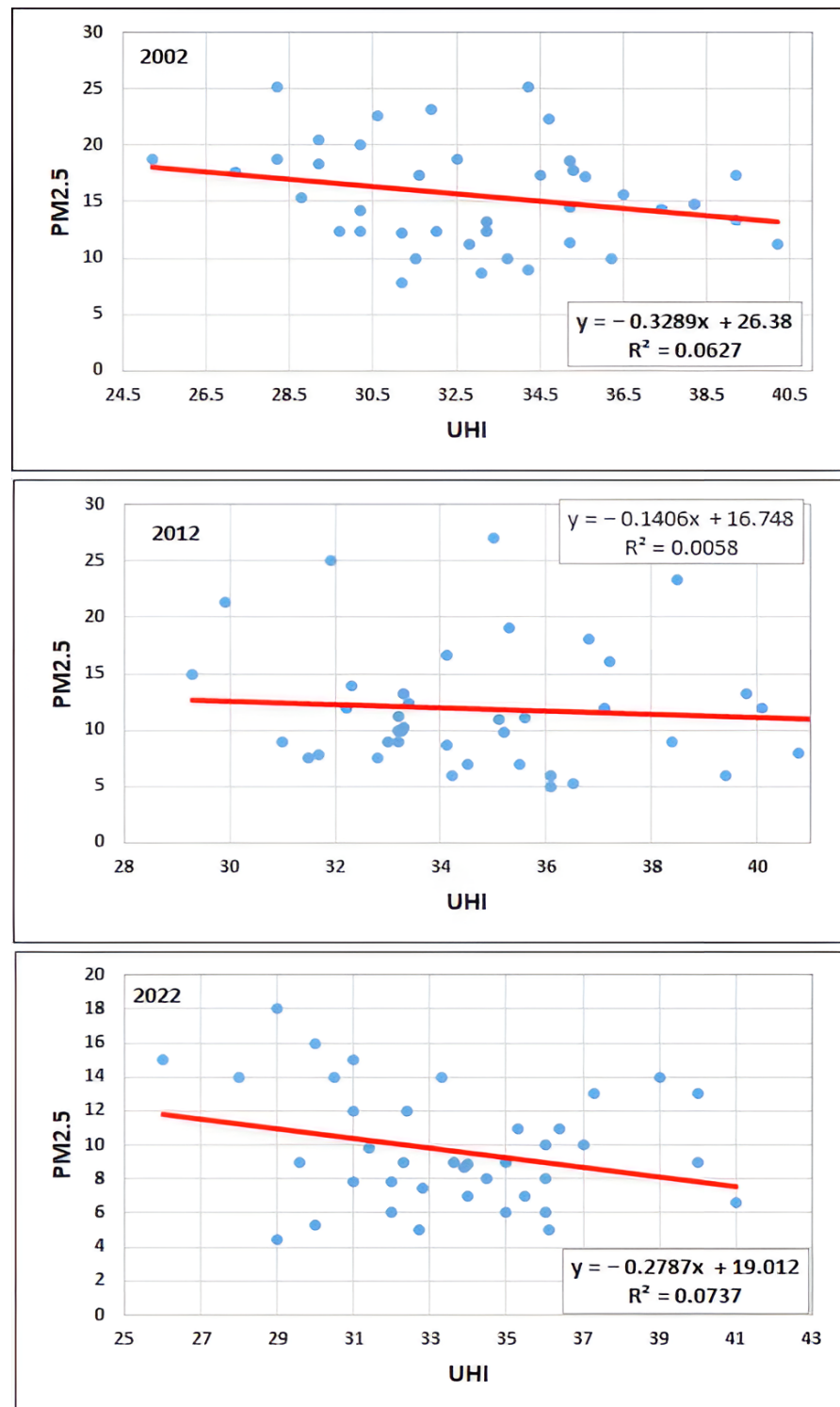


Figure 16. Scattered plots of UHI and PM2.5 of the three Cities during 2002, 2012, and 2022.

4. Discussion

The purpose of this study was to examine the connection between PM2.5 and UHI in Alabama’s metropolitan cities, focusing on the spatiotemporal variations of these phenomena. The study analyzed the factors contributing to PM2.5 concentrations in both urban and rural agricultural interface areas, taking into account the geographical differences between the cities. The study’s three key findings were: accurate measurements of LULC, LST, NDBI, and PM2.5 trends across Alabama’s urban centers, evidence of significant UHI intensity

during the study period, highlighting the importance of anthropogenic heat-generating activities for UHI, and correlations between all parameters influencing PM_{2.5} concentrations. The study's results provide a preliminary approach to understanding the link between UHI and the concentration of PM_{2.5} in these cities. Further research is needed to explore the exact correlation between UHI and PM_{2.5}, especially during the COVID-19 lockdown when fewer human activities are happening. Additionally, the COVID-19 lockdown period demonstrates the significance of the mutual urban-rural effect on UHI intensity by showing a decrease in PM_{2.5} concentrations. The lockdown significantly restricted human activity, simulating a well-controlled study on the interaction between people, environment, and atmosphere.

The investigation of PM_{2.5}'s spatial and temporal distribution features was challenging due to the uneven coverage of ground monitoring sites. Data collection occurred on a day with cloud coverage below 15%, and weather conditions, particularly rain, had a significant impact on concentration. This study discovered that PM_{2.5} concentration decreased as the intensity of UHI increased, which is influenced by thermally induced air circulation and changes in boundary-layer height as a result of urbanization. Urbanization is a significant contributor to rising temperatures, with LULC patterns, building geometry, and anthropogenic heat emissions all playing a role. The study analyzed LULC, LST, NDBI, and PM_{2.5} trends across Alabama's urban cities, providing precise measurements and insights into the impact of urbanization on the environment.

The study discovered that human activities hurt the environment in cities. The natural surroundings of urban areas are altered by artificial materials like concrete and radiation absorption materials, which impact heat exchange and the microclimate. The Urban Heat Island (UHI) effect occurs when Land Use Land Cover (LULC) characteristics alter due to urbanization. Swift population and economic growth, along with high energy consumption, are the primary factors identified for urban climate change in Alabama's metropolitan cities, causing noteworthy PM_{2.5} emissions. Human activities such as transportation, manufacturing, and the use of cooling and heating systems in Birmingham, Montgomery, and Mobile cities have a significant impact on increasing LST and UHIs. These activities consume substantial energy, producing additional anthropogenic heat, further increasing LST and UHIs.

Even though the forest areas in the three cities make up more than 70% of their total area, changes in land use and land cover (LULC) have had a significant impact on the land surface temperature (LST). This study discovered that the urban areas of the cities have grown between 2002 and 2022, resulting in increased areas covered by asphalt such as built-up areas, manufacturing areas, and roadways, which have extended to the urban-rural interface. The study also predicts that this expansion is likely to continue in the future. These findings are consistent with previous research cited in references [10,14,15,35,74,75].

A significant finding is that urbanization and the resulting changes in land use and cover have caused an increase in land surface temperature (LST), which has led to the loss of vegetation. This loss of vegetation is crucial in regulating LST. The study has shown that having vegetation, such as healthy green spaces and forests, can reduce LST and help decrease PM_{2.5} concentrations in the future. These results are consistent with previous research studies [5,35,67,68].

Over the past thirty years, there has been a significant increase in the urbanization rate of Birmingham, Montgomery, and Mobile. Between 2002 and 2022, the built-up area of these cities grew by around 20%, 27%, and 34% respectively. This growth is mainly due to the transformation of forests and croplands into open land, which eventually became built-up areas. This reflects the expansion and diversification of the cities' economies. To tackle these changes, the cities have implemented a master plan that focuses on improving infrastructure, revitalizing the economy, and reconnecting communities to the riverside. However, rapid urbanization has also hurt the urban environmental quality, resulting in rising UHI. This study's findings could aid in reducing the UHI while enhancing the urban environmental quality, which is in line with previous research [9,16,18,32,34,35,55,71,76–82].

According to Table 5, the Urban Heat Island Intensity (UHII) is significantly higher in urban areas like Birmingham, Montgomery, and Mobile compared to rural agricultural areas. This is because the rural areas have more vegetation, while urban areas have expanded and developed extensively in the past 30 years, resulting in the UHI effect. From 2002 to 2022, Birmingham and Montgomery experienced a significant increase in UHI, with the highest concentration in downtown areas and moderate to high concentrations in the northeastern and southern regions. Similarly, Mobile saw a notable increase in UHI from 2012 to 2022, with concentrations in the northeastern, southwestern, and central parts of the city. Table 5 shows that this pattern remained consistent throughout the study period, demonstrating the UHI phenomenon in these cities compared to their rural counterparts. In summary, these cities have higher temperatures than their rural areas due to the interaction of solar radiation with urban materials like cement, asphalt, and minerals, which differs from how it interacts with land cover in agricultural areas. The absorbed solar radiation in urban areas raises the temperature, while various urban surfaces re-emit this radiation as sensible heat flux, resulting in a higher UHI [4,35,72,83,84]. This mechanism is different in agricultural areas due to the dense land cover of forests and soil moisture, which absorbs solar radiation through the process of evaporation transpiration, converting it into latent heat with no thermal return [24,47,69,83,85].

Table 5. Diurnal UHI intensity in Birmingham, Montgomery, and Mobile and its rural boundaries during 2002–2022.

City	Diurnal LST °C 2002–2022			Diurnal LST °C 2012–2022			Diurnal LST °C 2002–2022		
	Urban	Rural	UHI Intensity	Urban	Rural	UHI Intensity	Urban	Rural	UHI Intensity
Birmingham	37.3	35.4	1.9	38.4	35.8	2.6	41	37.4	3.6
Montgomery	38.2	34.8	3.4	39.9	36.4	3.5	42.1	38.6	3.5
Mobile	38.1	35.5	2.6	39.6	36.2	3.4	42.6	38.7	3.9

Source: GIS Spatial Zonal Analysis to Landsat images 2002, 2012, and 2022.

After analyzing the data, it has been determined that Birmingham, Montgomery, and Mobile are experiencing increased warmth. These cities also have higher exposure risk, which matches findings from previous studies in the same region. The current study has discovered that there are notable differences in land surface temperatures (LST) between urban and rural agricultural interface areas. The results demonstrate that the urban areas in the three cities examined have higher LST compared to the rural agricultural interface areas. This is attributed to human activities and urban expansion in urban areas, whereas rural areas benefit from natural vegetation cover and forests that help to lower temperatures and absorb solar radiation. These results are consistent with previous research on the urban heat island effect (UHI) [3,6,34,37,39,48,70,81–83,85–88].

It’s worth noting that the urban heat island effect was more pronounced in 2012 and 2022 than in 2002 for all three cities. Mobile had the highest recorded land surface temperature (LST), followed by Birmingham, whereas Montgomery had the lowest urban heat island (UHI) in 2022. However, in 2012, Birmingham’s UHI was greater than Montgomery and Mobile. The study also found that the average temperature in summer 2022 was 35.5 °C and 37 °C for the downtown station in Mobile and the airport station in Birmingham, respectively. Interestingly, the average temperature was 33.3 °C and 31.5 °C in Birmingham and Mobile, respectively, as depicted in Figure 17. Furthermore, the study discovered a positive correlation between fine PM2.5 and land use/land cover change (LULC), particularly with urban areas and LST, with a correlation coefficient exceeding 0.7.

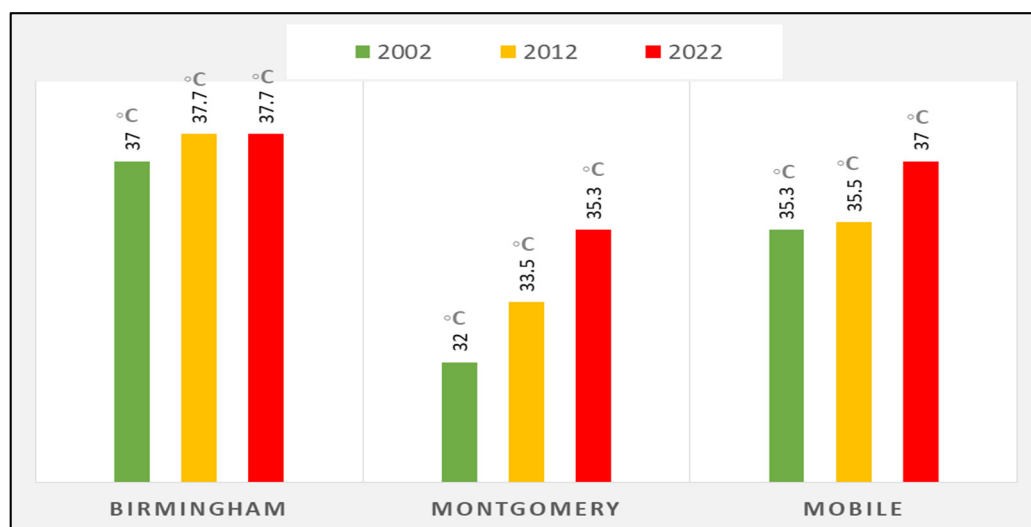


Figure 17. LST variations in the three cities during summer over 2002, 2012, and 2022.

The results of this study were surprising, as it revealed a notable reduction in PM2.5 levels in three cities during the period from 2002 to 2022. Throughout the years under examination, each city achieved an acceptable R2 value, with readings of 0.06, 0.77, and 0.01, demonstrating a significant link between UHI temperature and PM2.5 concentrations. Furthermore, the study determined a robust and unfavorable correlation between LST and PM2.5 levels in Birmingham, Montgomery, and Mobile in 2002, 2012, and 2022 (refer to Figure 6).

The results could be attributed to various factors. Firstly, the weather in Alabama is characterized by precipitation throughout the year and is influenced by different air masses, including the warm and humid air from the Gulf of Mexico in subtropical latitudes. Consequently, the three cities under investigation frequently receive heavy rainfall, which helps to clean the air of suspended pollutants, despite increased human activity. Secondly, the research findings revealed that Birmingham, Montgomery, and Mobile have high levels of human activity in both urban and rural areas. Surprisingly, interruptions to this activity, as seen during the COVID-19 lockdown period, led to a decrease in PM2.5 concentrations and an increase in the Urban Heat Island effect. The COVID-19 lockdowns provided a well-controlled study on the interplay between people, environment, and atmosphere.

To better estimate future scenarios of the Urban Heat Island (UHI) phenomenon [74], it is important to consider human interactions within the surrounding areas of the three cities. Although the decrease in PM2.5 concentrations during the COVID-19 lockdown can be attributed to this factor, it is not a long-term solution. Alabama's cities like Birmingham, Montgomery, and Mobile are situated amidst vast areas of forests and natural vegetation which cover around 70% of the state. The forest trees in these areas can reduce PM2.5 concentrations by absorbing them during photosynthesis and transpiration processes, as well as via physical adsorption onto leaf surfaces. Additionally, physiological processes, such as maximum assimilation and carboxylation rates, have also been found to reduce PM2.5 concentrations. These findings are supported by numerous previous studies [56,73,89–92].

To clarify, maintaining healthy vegetation cover can reduce PM2.5 levels in several ways, including collecting and filtering air particles through leaf pubescence and stomata. Among different types of vegetation, shrublands have the greatest impact on PM2.5 concentrations, followed by grasslands and forests. These findings can help better understand the factors that contribute to the urban heat island effect in Alabama. For instance, the study confirms the crucial role forests play in reducing PM2.5 concentrations, which could aid state authorities in protecting these valuable natural resources.

5. The Study Limitations

Due to Alabama's subtropical climate, the study encountered difficulty in obtaining adequate satellite imagery for the desired timeframe. The region experiences heavy cloud cover of over 90% for most days of the year, with only a few days in the summer seeing a drop to 15%. This presents a challenge in accurately assessing seasonal variations in both LST and PM2.5. To evaluate the impact of urban heat islands, the study used surface temperature as a proxy for air temperature. Landsat 8 captured the images used in the study, hovering over a location for a specific period. Each image portrayed a specific day and period during the summer months.

6. Conclusions

The study conducted a thorough analysis of the variation of summertime urban heat island (UHI) and its correlation with PM2.5 in Metropolitan Cities in Alabama. In addition, it used Landsat imagery and PM2.5 data to investigate the changes in Land Surface Temperature (LST) in relation to Land Use/Land Cover (LULC) classes and its impact on PM2.5 in urban and urban-agricultural areas. Moreover, it examined the changes in LULC from 2002 to 2022 to determine the extent of areas affected by UHI and its influence on LST in three cities in Alabama.

The research discovered that between 2002 and 2022, urbanization and human activity increased due to urban expansion, while forest and cropland areas decreased. As a result, there was a notable accumulation of LST in cities and their surrounding regions, leading to variations in LST levels at different times and locations. The study also revealed that changes in LULC affected urban climates in these cities and their surroundings. Over the past thirty years, the built-up area has increased significantly, while forests, cropland, and water bodies have declined dramatically. In Birmingham, Montgomery, and Mobile cities, the average LST difference was 3.90, 3.20, and 3.80 °C respectively. Furthermore, the mean LST rose by 1.4 °C per decade, indicating a rise in the influence of the UHI phenomenon over time.

The study found that there was a positive correlation between LST and NDBI, and a negative correlation between LST and PM2.5 concentrations in Mobile, Birmingham, and Montgomery from 2002 to 2022. The results of LULC and NDBI indicated that rapid urbanization occurred in these cities. The R^2 values showed that there was a negative correlation between PM2.5 concentrations and UHI intensity, while the correlation between UHI intensity and NDBI was positive. The study also found that PM2.5 concentrations had been decreasing annually since 2002, which significantly improved air quality. However, LST remained consistently high throughout the study period. Despite the dominant LULC type, PM2.5 concentrations in these cities decreased from 2002 to 2022. This suggests that the contribution of urban areas to climate change has decreased, contrary to expectations that rising temperatures would lead to increased pollutant concentrations. The study concluded that the upward trend of LST in metropolitan areas in Alabama was higher than that of the urban-agricultural interface. These results may be explained by the state's unique geographic characteristics, hot and humid subtropical climate with year-round heavy rainfall, and the decrease in pollutants during the COVID-19 lockdown in 2019.

The intensity and spatiotemporal extent of urban heat island (UHI) characteristics and their correlation with PM2.5 concentrations are influenced by various physical factors such as healthy vegetation, forest cover, local climate, and environmental conditions, as well as human factors such as land use, NDBI, and COVID-19 lockdown. These determinants play a significant role in explaining the land-atmosphere interaction processes in metropolitan cities.

Author Contributions: Conceptualization, G.E.A.; Software, H.I.; Validation, G.E.A.; Formal analysis, G.E.A.; Resources, G.E.A. and H.I.; Writing—original draft, H.I.; Writing—review & editing, G.E.A.; Project administration, G.E.A. All authors have read and agreed to the published version of the manuscript.

Funding: This research received no specific grant from any funding agency in the public, commercial, or not-for-profit sectors.

Data Availability Statement: The datasets generated and/or analyzed during this study are available from the corresponding author upon reasonable request.

Conflicts of Interest: The authors declare no conflict of interest.

Appendix A

$$TOA\ Radiance = MLQ_{cal} + AL \quad (A1)$$

where:

TOA Radiance: Top of Atmosphere radiance

MLQ_{cal}: DN value of pixel for radiance

AL: The maximum radiance

$$TOA\ Reflectance = M\rho Q_{cal} + A\rho \quad (A2)$$

where:

TOA Reflectance: Top of Atmosphere

MLQ_{cal}: DN value of pixel for reflectance

A ρ : The maximum reflectance

$$L\lambda = L_{max} - L_{min} * Q_{cal} / (Q_{calmax} - Q_{calmin}) + L_{min} - O_i \quad (A3)$$

where:

L λ : Spectral radiance

L_{max}: Maximum radiance

L_{min}: Minimum radiance

Q_{cal}: DN value of the pixel

Q_{calmax}: DN value of pixel maximum

Q_{calmin}: DN value of pixel minimum

O_i: Correction value for bands 6 and 10

After converting DN values to at-sensor spectral radiance, the band data (6 and 10) should be converted to brightness temperature (BT) using the thermal constants given in the metadata file through the following equation:

$$BT = K2 \ln(K1 / L\lambda) + 1 - 273.15 \quad (A4)$$

where:

K1 and K2 are the thermal constants of Radiance of bands 10 and 6 which can be identified in the metadata file associated with the satellite image.

L λ : Spectral radiance

Normalized Difference Vegetation Index (NDVI) is important to identify different land cover types of the studied areas. NDVI ranges between -1.0 to $+1.0$. NDVI is calculated based on the normalized difference between the red band (0.64–0.67 μm) and near-infrared band (0.85–0.88 μm) of the images using the equation:

$$NDVI = \frac{NIR - RED}{NIR + RED} \quad (A5)$$

The next step is to calculate the proportional vegetation (P_v) and emissivity (ϵ) as the calculation of NDVI is especially important for both. Proportional vegetation (P_v) from NDVI values obtained by the estimation of areas under each land cover type. It depends on the values of vegetation and bare soil proportions acquired from the NDVI of pure pixels as its values of NDVI_v = 0.5 and NDVI_s = 0.2 were proposed to apply in global conditions.

On the other hand, the value for vegetated surfaces ($NDVI_v = 0.5$) may be too low in some cases, for higher resolution data in the agricultural sites, $NDVI_v$ so can reach 0.8 or 0.9. P_v can be calculated using the following equation:

$$P_v = (NDVI - NDVI_s / NDVI_v - NDVI_s)2 \quad (A6)$$

The calculation of Land Surface emissivity (LSE) is used to calculate the LST (Land Surface Temperature), as LSE is a proportionality factor that measures the radiance of a black body (Planck's law) to analyze the emitted radiance and the ability to spread thermal energy crossways the surface into the atmosphere (Ugur and Gordana, 2016). It is calculated through the following:

$$\epsilon\lambda = \epsilon_v\lambda P_v + \epsilon_s\lambda(1 - P_v) + C\lambda \quad (A7)$$

where,

ϵ_v : Vegetation emissivity

ϵ_s : Soil emissivity

C: Surface roughness

The average emissivity of four major land cover types can be considered in Band 6 and 10 as, when the NDVI is less than 0, it is classified as water. If the emissivity value of 0.991 for NDVI values between 0 and 0.2, it is considered that the land cover type is soil. The emissivity value of 0.966 is assigned values between 0.2 and 0.5 are considered a mixture of soil and vegetation cover. In the last case, when the NDVI value is greater than 0.5, it is considered vegetation cover, and the value of 0.973 is assigned.

The last step is to calculate LST by using the brightness temperature (BT) of bands 6 and 10. Besides LSE is derived from P_v and NDVI (Stathopoulos and Cartalis, 2007). It can be calculated through this equation:

$$T_s = BT / \{1 + \lambda BT \ln \epsilon\lambda\} \quad (A8)$$

where,

T_s : LST in Celsius ($^{\circ}\text{C}$).

BT: sensor BT ($^{\circ}\text{C}$).

λ : Average wavelength of bands 6 and 10.

$\epsilon\lambda$ Emissivity and ρ is ($h \times$) which is equal to 1.438×10^{-2} m/K.

σ is the Boltzmann constant (1.38×10^{-23} J/K).

h is Planck's constant (6.626×10^{-34}).

c is the velocity of light (3×10^8 m/s).

The calculation of UHI (Urban Heat Island) is estimated through LST in the following equation:

$$UHI = \sigma + \mu/2 \quad (A9)$$

where,

UHI: Urban Heat Island.

LST: Land Surface Temperature

Calculation of Urban Heat Island (UHI) Intensity: It is defined as the temperature difference between urban and rural places (or areas), $\Delta T_{u-r} = T_u - T_r$, where ΔT_{u-r} is UHI intensity, T_u is urban temperature, and T_r is rural temperature. We calculated the temperature of the urban and the rural areas through the observed data mentioned on the website ([AirNow.gov](https://airnow.gov)) and it collected by the stations whose responsibility is the meteorological data for both the urban and rural areas the following (Table 3) will show the urban area, rural area and the stations for collection the meteorological data:

$$\Delta T_{u-r} = T_u - T_r \quad (A10)$$

where,

$\Delta Tu-r$: UHI intensity

Tu: Urban Temperature

Tr: Rural Temperature

Appendix B

Table A1. Urban and rural stations in study area.

Urban Area	Rural Area	Name of Station	Location of Station
Montgomery	Pike	Montgomery Airport AL,	32.29 N–86.40 W
Birmingham	Shelby	Alabaster Shelby Co Air	33.17 N–86.78 W
Mobile	Baldwin	Fairhope 3 NE, AL	30.54 N–87.87 W

Table A2 shows a linear correlation between UHI intensity temperature and NDBI in the three cities during the specified periods (2002, 2012, and 2022) in summer. It is noticed that the values of R^2 ranged between 0.80 and 0.95. Therefore, there is a strong positive correlation observed between UHI intensity and NDBI in the three cities representing the study areas. As a result, NDBI has a significant correlation with UHI.

Table A2. The liner correlation between UHI intensity and NDBI in three cities during 2002–2022.

City	R^2 Value		
	2002	2012	2022
Birmingham	0.89	0.93	0.95
Montgomery	0.85	0.89	0.92
Mobile	0.80	0.92	0.93

References

- Bettencourt, L.M.A. Urban Growth and the Emergent Statistics of Cities. *Sci. Adv.* **2020**, *6*, eaat8812. [[CrossRef](#)] [[PubMed](#)]
- Wang, J.; Yan, Z.-W. Urbanization-Related Warming in Local Temperature Records: A Review. *Atmos. Ocean. Sci. Lett.* **2016**, *9*, 129–138. [[CrossRef](#)]
- Ranagalage, M.; Ratnayake, S.S.; Dissanayake, D.; Kumar, L.; Wickremasinghe, H.; Vidanagama, J.; Cho, H.; Udagedara, S.; Jha, K.K.; Simwanda, M.; et al. Spatiotemporal Variation of Urban Heat Islands for Implementing Nature-Based Solutions: A Case Study of Kurunegala, Sri Lanka. *ISPRS Int. J. Geo-Inf.* **2020**, *9*, 461. [[CrossRef](#)]
- Dutta, D.; Rahman, A.; Paul, S.K.; Kundu, A. Impervious Surface Growth and Its Inter-Relationship with Vegetation Cover and Land Surface Temperature in Peri-Urban Areas of Delhi. *Urban Clim.* **2021**, *37*, 100799. [[CrossRef](#)]
- Buo, I.; Sagris, V.; Burdun, I.; Uuemaa, E. Estimating the Expansion of Urban Areas and Urban Heat Islands (UHI) in Ghana: A Case Study. *Nat. Hazards* **2021**, *105*, 1299–1321. [[CrossRef](#)]
- Shi, L.; Chu, E.; Anguelovski, I.; Aylett, A.; Debats, J.; Goh, K.; Schenk, T.; Seto, K.C.; Dodman, D.; Roberts, D.; et al. Roadmap towards Justice in Urban Climate Adaptation Research. *Nat. Clim. Chang.* **2016**, *6*, 131–137. [[CrossRef](#)]
- Du, P.; Chen, J.; Bai, X.; Han, W. Understanding the Seasonal Variations of Land Surface Temperature in Nanjing Urban Area Based on Local Climate Zone. *Urban Clim.* **2020**, *33*, 100657. [[CrossRef](#)]
- McDonnell, M.J.; MacGregor-Fors, I. The ecological future of cities. *Science* **2016**, *352*, 936–938. [[CrossRef](#)]
- Naim, N.H.; Kafy, A.-A. Assessment of Urban Thermal Field Variance Index and Defining the Relationship between Land Cover and Surface Temperature in Chattogram City: A Remote Sensing and Statistical Approach. *Environ. Chall.* **2021**, *4*, 100107. [[CrossRef](#)]
- Liu, P.; Jia, S.; Han, R.; Liu, Y.; Lu, X.; Zhang, H. RS and GIS Supported Urban LULC and UHI Change Simulation and Assessment. *J. Sens.* **2020**, *2020*, 5863164. [[CrossRef](#)]
- Martilli, A.; Krayerhoff, E.S.; Nazarian, N. Is the Urban Heat Island Intensity Relevant for Heat Mitigation Studies? *Urban Clim.* **2020**, *31*, 100541. [[CrossRef](#)]
- Qiao, Z.; Lu, Y.; He, T.; Wu, F.; Xu, X.; Liu, L.; Wang, F.; Sun, Z.; Han, D. Spatial Expansion Paths of Urban Heat Islands in Chinese Cities: Analysis from a Dynamic Topological Perspective for the Improvement of Climate Resilience. *Resour. Conserv. Recycl.* **2023**, *188*, 106680. [[CrossRef](#)]

13. Atasoy, M. Assessing the Impacts of Land-Use/Land-Cover Change on the Development of Urban Heat Island Effects. *Environ. Dev. Sustain.* **2020**, *22*, 7547–7557. [[CrossRef](#)]
14. Shahfahad; Rihan, M.; Naikoo, M.W.; Ali, M.A.; Usmani, T.M.; Rahman, A. Urban Heat Island Dynamics in Response to Land-Use/Land-Cover Change in the Coastal City of Mumbai. *J. Indian Soc. Remote Sens.* **2021**, *49*, 2227–2247. [[CrossRef](#)]
15. Shahfahad; Talukdar, S.; Rihan, M.; Hang, H.T.; Bhaskaran, S.; Rahman, A. Modelling Urban Heat Island (UHI) and Thermal Field Variation and Their Relationship with Land Use Indices over Delhi and Mumbai Metro Cities. *Environ. Dev. Sustain.* **2022**, *24*, 3762–3790. [[CrossRef](#)]
16. Stowell, J.D.; Bi, J.; Al-Hamdan, M.Z.; Lee, H.J.; Lee, S.-M.; Freedman, F.; Kinney, P.L.; Liu, Y. Estimating PM_{2.5} in Southern California Using Satellite Data: Factors That Affect Model Performance. *Environ. Res. Lett.* **2020**, *15*, 094004. [[CrossRef](#)]
17. Wang, Y.; Du, H.; Xu, Y.; Lu, D.; Wang, X.; Guo, Z. Temporal and Spatial Variation Relationship and Influence Factors on Surface Urban Heat Island and Ozone Pollution in the Yangtze River Delta, China. *Sci. Total Environ.* **2018**, *631–632*, 921–933. [[CrossRef](#)]
18. Li, H.; Meier, F.; Lee, X.; Chakraborty, T.; Liu, J.; Schaap, M.; Sodoudi, S. Interaction between Urban Heat Island and Urban Pollution Island during Summer in Berlin. *Sci. Total Environ.* **2018**, *636*, 818–828. [[CrossRef](#)]
19. Guo, G.; Zhou, X.; Wu, Z.; Xiao, R.; Chen, Y. Characterizing the Impact of Urban Morphology Heterogeneity on Land Surface Temperature in Guangzhou, China. *Environ. Model. Softw.* **2016**, *84*, 427–439. [[CrossRef](#)]
20. Yang, G.; Ren, G.; Zhang, P.; Xue, X.; Tysa, S.K.; Jia, W.; Qin, Y.; Zheng, X.; Zhang, S. PM_{2.5} Influence on Urban Heat Island (UHI) Effect in Beijing and the Possible Mechanisms. *Geophys. Res. Atmos.* **2021**, *126*, e2021JD035227. [[CrossRef](#)]
21. Von Bismarck-Osten, C.; Birmili, W.; Ketzel, M.; Massling, A.; Petäjä, T.; Weber, S. Characterization of Parameters Influencing the Spatio-Temporal Variability of Urban Particle Number Size Distributions in Four European Cities. *Atmos. Environ.* **2013**, *77*, 415–429. [[CrossRef](#)]
22. Borge, R.; Narros, A.; Artiñano, B.; Yagüe, C.; Gómez-Moreno, F.J.; De La Paz, D.; Román-Cascón, C.; Díaz, E.; Maqueda, G.; Sastre, M.; et al. Assessment of Microscale Spatio-Temporal Variation of Air Pollution at an Urban Hotspot in Madrid (Spain) through an Extensive Field Campaign. *Atmos. Environ.* **2016**, *140*, 432–445. [[CrossRef](#)]
23. Zhao, L.; Oppenheimer, M.; Zhu, Q.; Baldwin, J.W.; Ebi, K.L.; Bou-Zeid, E.; Guan, K.; Liu, X. Interactions between Urban Heat Islands and Heat Waves. *Environ. Res. Lett.* **2018**, *13*, 034003. [[CrossRef](#)]
24. Yue, W.; Liu, X.; Zhou, Y.; Liu, Y. Impacts of Urban Configuration on Urban Heat Island: An Empirical Study in China Mega-Cities. *Sci. Total Environ.* **2019**, *671*, 1036–1046. [[CrossRef](#)]
25. Zhou, D.; Zhao, S.; Zhang, L.; Sun, G.; Liu, Y. The Footprint of Urban Heat Island Effect in China. *Sci. Rep.* **2015**, *5*, 11160. [[CrossRef](#)] [[PubMed](#)]
26. Giridharan, R.; Emmanuel, R. The Impact of Urban Compactness, Comfort Strategies and Energy Consumption on Tropical Urban Heat Island Intensity: A Review. *Sustain. Cities Soc.* **2018**, *40*, 677–687. [[CrossRef](#)]
27. Zhou, B.; Rybski, D.; Kropp, J.P. The Role of City Size and Urban Form in the Surface Urban Heat Island. *Sci. Rep.* **2017**, *7*, 4791. [[CrossRef](#)]
28. Kang, H.; Zhu, B.; De Leeuw, G.; Yu, B.; Van Der A, R.J.; Lu, W. Impact of Urban Heat Island on Inorganic Aerosol in the Lower Free Troposphere: A Case Study in Hangzhou, China. *Atmos. Chem. Phys.* **2022**, *22*, 10623–10634. [[CrossRef](#)]
29. Hinkel, K.M.; Nelson, F.E.; Klene, A.E.; Bell, J.H. The Urban Heat Island in Winter at Barrow, Alaska. *Int. J. Climatol.* **2003**, *23*, 1889–1905. [[CrossRef](#)]
30. Ackley, J.W.; Angilletta, M.J.; DeNardo, D.; Sullivan, B.; Wu, J. Urban Heat Island Mitigation Strategies and Lizard Thermal Ecology: Landscaping Can Quadruple Potential Activity Time in an Arid City. *Urban Ecosyst.* **2015**, *18*, 1447–1459. [[CrossRef](#)]
31. Tan, J.; Zheng, Y.; Tang, X.; Guo, C.; Li, L.; Song, G.; Zhen, X.; Yuan, D.; Kalkstein, A.J.; Li, F.; et al. The Urban Heat Island and Its Impact on Heat Waves and Human Health in Shanghai. *Int. J. Biometeorol.* **2010**, *54*, 75–84. [[CrossRef](#)] [[PubMed](#)]
32. Simwanda, M.; Ranagalage, M.; Estoque, R.C.; Murayama, Y. Spatial Analysis of Surface Urban Heat Islands in Four Rapidly Growing African Cities. *Remote Sens.* **2019**, *11*, 1645. [[CrossRef](#)]
33. Dian, C.; Pongrácz, R.; Dezső, Z.; Bartholy, J. Annual and Monthly Analysis of Surface Urban Heat Island Intensity with Respect to the Local Climate Zones in Budapest. *Urban Clim.* **2020**, *31*, 100573. [[CrossRef](#)]
34. Dissanayake, D.M.S.L.B.; Morimoto, T.; Ranagalage, M.; Murayama, Y. Land-Use/Land-Cover Changes and Their Impact on Surface Urban Heat Islands: Case Study of Kandy City, Sri Lanka. *Climate* **2019**, *7*, 99. [[CrossRef](#)]
35. Balew, A.; Semaw, F. Impacts of Land-Use and Land-Cover Changes on Surface Urban Heat Islands in Addis Ababa City and Its Surrounding. *Environ. Dev. Sustain.* **2022**, *24*, 832–866. [[CrossRef](#)]
36. Cheval, S.; Popa, A.-M.; Şandric, I.; Ioja, I.-C. Exploratory Analysis of Cooling Effect of Urban Lakes on Land Surface Temperature in Bucharest (Romania) Using Landsat Imagery. *Urban Clim.* **2020**, *34*, 100696. [[CrossRef](#)]
37. Roustai, I.; Sarif, M.; Gupta, R.; Olafsson, H.; Ranagalage, M.; Murayama, Y.; Zhang, H.; Mushore, T. Spatiotemporal Analysis of Land Use/Land Cover and Its Effects on Surface Urban Heat Island Using Landsat Data: A Case Study of Metropolitan City Tehran (1988–2018). *Sustainability* **2018**, *10*, 4433. [[CrossRef](#)]
38. Han, D.; Zhang, T.; Qin, Y.; Tan, Y.; Liu, J. A Comparative Review on the Mitigation Strategies of Urban Heat Island (UHI): A Pathway for Sustainable Urban Development. *Clim. Dev.* **2023**, *15*, 379–403. [[CrossRef](#)]
39. Shen, P.; Wang, M.; Liu, J.; Ji, Y. Hourly Air Temperature Projection in Future Urban Area by Coupling Climate Change and Urban Heat Island Effect. *Energy Build.* **2023**, *279*, 112676. [[CrossRef](#)]

40. Gedzelman, S.D.; Austin, S.; Cermak, R.; Stefano, N.; Partridge, S.; Quesenberry, S.; Robinson, D.A. Mesoscale Aspects of the Urban Heat Island around New York City. *Theor. Appl. Climatol.* **2003**, *75*, 29–42. [[CrossRef](#)]
41. Lokoshchenko, M.A.; Alekseeva, L.I. Influence of Meteorological Parameters on the Urban Heat Island in Moscow. *Atmosphere* **2023**, *14*, 507. [[CrossRef](#)]
42. Sofer, M.; Potchter, O. The Urban Heat Island of a City in an Arid Zone: The Case of Eilat, Israel. *Theor. Appl. Climatol.* **2006**, *85*, 81–88. [[CrossRef](#)]
43. Murata, A.; Sasaki, H.; Hanafusa, M.; Kurihara, K. Estimation of Urban Heat Island Intensity Using Biases in Surface Air Temperature Simulated by a Nonhydrostatic Regional Climate Model. *Theor. Appl. Clim.* **2013**, *112*, 351–361. [[CrossRef](#)]
44. Gao, Y.; Zhao, J.; Han, L. Exploring the Spatial Heterogeneity of Urban Heat Island Effect and Its Relationship to Block Morphology with the Geographically Weighted Regression Model. *Sustain. Cities Soc.* **2022**, *76*, 103431. [[CrossRef](#)]
45. Hu, D.; Meng, Q.; Schlink, U.; Hertel, D.; Liu, W.; Zhao, M.; Guo, F. How Do Urban Morphological Blocks Shape Spatial Patterns of Land Surface Temperature over Different Seasons? A Multifactorial Driving Analysis of Beijing, China. *Int. J. Appl. Earth Obs. Geoinf.* **2022**, *106*, 102648. [[CrossRef](#)]
46. Ivajnsič, D.; Kaligarič, M.; Žiberna, I. Geographically Weighted Regression of the Urban Heat Island of a Small City. *Appl. Geogr.* **2014**, *53*, 341–353. [[CrossRef](#)]
47. Zhang, L.; Shi, X.; Chang, Q. Exploring Adaptive UHI Mitigation Solutions by Spatial Heterogeneity of Land Surface Temperature and Its Relationship to Urban Morphology in Historical Downtown Blocks, Beijing. *Land* **2022**, *11*, 544. [[CrossRef](#)]
48. Xiang, Y.; Huang, C.; Huang, X.; Zhou, Z.; Wang, X. Seasonal Variations of the Dominant Factors for Spatial Heterogeneity and Time Inconsistency of Land Surface Temperature in an Urban Agglomeration of Central China. *Sustain. Cities Soc.* **2021**, *75*, 103285. [[CrossRef](#)]
49. Taha, H. Meso-Urban Meteorological and Photochemical Modeling of Heat Island Mitigation. *Atmos. Environ.* **2008**, *42*, 8795–8809. [[CrossRef](#)]
50. Weng, Q.; Fu, P. Modeling Diurnal Land Temperature Cycles over Los Angeles Using Downscaled GOES Imagery. *ISPRS J. Photogramm. Remote Sens.* **2014**, *97*, 78–88. [[CrossRef](#)]
51. Vahmani, P.; Ban-Weiss, G.A. Impact of Remotely Sensed Albedo and Vegetation Fraction on Simulation of Urban Climate in WRF-Urban Canopy Model: A Case Study of the Urban Heat Island in Los Angeles: Satellite-Supported Urban Climate Model. *J. Geophys. Res. Atmos.* **2016**, *121*, 1511–1531. [[CrossRef](#)]
52. Bornstein, R.; Lin, Q. Urban Heat Islands and Summertime Convective Thunderstorms in Atlanta: Three Case Studies. *Atmos. Environ.* **2000**, *34*, 507–516. [[CrossRef](#)]
53. Chun, B.; Guhathakurta, S. Daytime and Nighttime Urban Heat Islands Statistical Models for Atlanta. *Environ. Plan. B Urban Anal. City Sci.* **2017**, *44*, 308–327. [[CrossRef](#)]
54. Lo, C.P.; Quattrochi, D.A. Land-Use and Land-Cover Change, Urban Heat Island Phenomenon, and Health Implications: A Remote Sensing Approach. *Photogramm. Eng. Remote Sens.* **2003**, *69*, 1053–1063. [[CrossRef](#)]
55. Liao, D.; Zhu, H.; Jiang, P. Study of Urban Heat Island Index Methods for Urban Agglomerations (Hilly Terrain) in Chongqing. *Theor. Appl. Clim.* **2021**, *143*, 279–289. [[CrossRef](#)]
56. Ying, Q.; Wu, L.; Zhang, H. Local and Inter-Regional Contributions to PM_{2.5} Nitrate and Sulfate in China. *Atmos. Environ.* **2014**, *94*, 582–592. [[CrossRef](#)]
57. Zhang, H.; Hu, J.; Kleeman, M.; Ying, Q. Source Apportionment of Sulfate and Nitrate Particulate Matter in the Eastern United States and Effectiveness of Emission Control Programs. *Sci. Total Environ.* **2014**, *490*, 171–181. [[CrossRef](#)]
58. Kim, Y.-H.; Baik, J.-J. Daily Maximum Urban Heat Island Intensity in Large Cities of Korea. *Theor. Appl. Clim.* **2004**, *79*, 151–164. [[CrossRef](#)]
59. Khorrami, B.; Gunduz, O. Spatio-Temporal Interactions of Surface Urban Heat Island and Its Spectral Indicators: A Case Study from Istanbul Metropolitan Area, Turkey. *Environ. Monit. Assess.* **2020**, *192*, 386. [[CrossRef](#)]
60. Peng, S.; Feng, Z.; Liao, H.; Huang, B.; Peng, S.; Zhou, T. Spatial-Temporal Pattern of, and Driving Forces for, Urban Heat Island in China. *Ecol. Indic.* **2019**, *96*, 127–132. [[CrossRef](#)]
61. Xiang, Y.; Cen, Q.; Peng, C.; Huang, C.; Wu, C.; Teng, M.; Zhou, Z. Surface Urban Heat Island Mitigation Network Construction Utilizing Source-Sink Theory and Local Climate Zones. *Build. Environ.* **2023**, *243*, 110717. [[CrossRef](#)]
62. Geng, X.; Zhang, D.; Li, C.; Yuan, Y.; Yu, Z.; Wang, X. Impacts of Climatic Zones on Urban Heat Island: Spatiotemporal Variations, Trends, and Drivers in China from 2001–2020. *Sustain. Cities Soc.* **2023**, *89*, 104303. [[CrossRef](#)]
63. Li, Y.; Sun, Y.; Li, J.; Gao, C. Socioeconomic Drivers of Urban Heat Island Effect: Empirical Evidence from Major Chinese Cities. *Sustain. Cities Soc.* **2020**, *63*, 102425. [[CrossRef](#)]
64. Meng, F.; Ren, G.; Zhang, R. Impacts of UHI on Heating and Cooling Loads in Residential Buildings in Cities of Different Sizes in Beijing–Tianjin–Hebei Region in China. *Atmosphere* **2023**, *14*, 1193. [[CrossRef](#)]
65. Sabrin, S.; Karimi, M.; Nazari, R. Modeling Heat Island Exposure and Vulnerability Utilizing Earth Observations and Social Drivers: A Case Study for Alabama, USA. *Build. Environ.* **2022**, *226*, 109686. [[CrossRef](#)]
66. Abbas, W.; Ismael, H. Assessment of Constructing Canopy Urban Heat Island Temperatures from Thermal Images: An Integrated Multi-Scale Approach. *Sci. Afr.* **2020**, *10*, e00607. [[CrossRef](#)]
67. Wang, Z.; Shafieezadeh, A. ESC: An Efficient Error-Based Stopping Criterion for Kriging-Based Reliability Analysis Methods. *Struct. Multidiscip. Optim.* **2019**, *59*, 1621–1637. [[CrossRef](#)]

68. Xu, C.; Wang, J.; Hu, M.; Wang, W. A New Method for Interpolation of Missing Air Quality Data at Monitor Stations. *Environ. Int.* **2022**, *169*, 107538. [[CrossRef](#)]
69. Wei, P.; Xie, S.; Huang, L.; Liu, L.; Tang, Y.; Zhang, Y.; Wu, H.; Xue, Z.; Ren, D. Spatial Interpolation of PM_{2.5} Concentrations during Holidays in South-Central China Considering Multiple Factors. *Atmos. Pollut. Res.* **2022**, *13*, 101480. [[CrossRef](#)]
70. Yang, J.; Zhao, Y.; Zou, Y.; Xia, D.; Lou, S.; Liu, W.; Ji, K. Effects of Tree Species and Layout on the Outdoor Thermal Environment of Squares in Hot-Humid Areas of China. *Buildings* **2022**, *12*, 1867. [[CrossRef](#)]
71. Tang, Y.; Xie, S.; Huang, L.; Liu, L.; Wei, P.; Zhang, Y.; Meng, C. Spatial Estimation of Regional PM_{2.5} Concentrations with GWR Models Using PCA and RBF Interpolation Optimization. *Remote Sens.* **2022**, *14*, 5626. [[CrossRef](#)]
72. Ghosh, S.; Kumar, D.; Kumari, R. Assessing Spatiotemporal Dynamics of Land Surface Temperature and Satellite-Derived Indices for New Town Development and Suburbanization Planning. *Urban Gov.* **2022**, *2*, 144–156. [[CrossRef](#)]
73. Kim, K.; Jeon, J.; Jung, H.; Kim, T.K.; Hong, J.; Jeon, G.-S.; Kim, H.S. PM_{2.5} Reduction Capacities and Their Relation to Morphological and Physiological Traits in 13 Landscaping Tree Species. *Urban For. Urban Green.* **2022**, *70*, 127526. [[CrossRef](#)]
74. Wu, H.; Wang, T.; Wang, Q.; Cao, Y.; Qu, Y.; Nie, D. Radiative Effects and Chemical Compositions of Fine Particles Modulating Urban Heat Island in Nanjing, China. *Atmos. Environ.* **2021**, *247*, 118201. [[CrossRef](#)]
75. Sheridan, S.C. A Survey of Public Perception and Response to Heat Warnings across Four North American Cities: An Evaluation of Municipal Effectiveness. *Int. J. Biometeorol.* **2007**, *52*, 3–15. [[CrossRef](#)]
76. Masson, V. Urban Surface Modeling and the Meso-Scale Impact of Cities. *Theor. Appl. Climatol.* **2006**, *84*, 35–45. [[CrossRef](#)]
77. Pal, S.; Xueref-Remy, I.; Ammoura, L.; Chazette, P.; Gibert, F.; Royer, P.; Dieudonné, E.; Dupont, J.-C.; Haeffelin, M.; Lac, C.; et al. Spatio-Temporal Variability of the Atmospheric Boundary Layer Depth over the Paris Agglomeration: An Assessment of the Impact of the Urban Heat Island Intensity. *Atmos. Environ.* **2012**, *63*, 261–275. [[CrossRef](#)]
78. Fallmann, J.; Forkel, R.; Emeis, S. Secondary Effects of Urban Heat Island Mitigation Measures on Air Quality. *Atmos. Environ.* **2016**, *125*, 199–211. [[CrossRef](#)]
79. Balew, A.; Korme, T. Monitoring Land Surface Temperature in Bahir Dar City and Its Surrounding Using Landsat Images. *Egypt. J. Remote Sens. Space Sci.* **2020**, *23*, 371–386. [[CrossRef](#)]
80. Shirangi, A.; Nieuwenhuijsen, M.; Vienneau, D.; Holman, C.D.J. Living near Agricultural Pesticide Applications and the Risk of Adverse Reproductive Outcomes: A Review of the Literature. *Paediatr. Perinat. Epidemiol.* **2011**, *25*, 172–191. [[CrossRef](#)]
81. Guha, S.; Govil, H.; Gill, N.; Dey, A. Analytical Study on the Relationship between Land Surface Temperature and Land Use/Land Cover Indices. *Ann. GIS* **2020**, *26*, 201–216. [[CrossRef](#)]
82. Zekar, A.; Milojevic-Dupont, N.; Zumwald, M.; Wagner, F.; Creutzig, F. Urban Form Features Determine Spatio-Temporal Variation of Ambient Temperature: A Comparative Study of Three European Cities. *Urban Clim.* **2023**, *49*, 101467. [[CrossRef](#)]
83. Kumari, P.; Garg, V.; Kumar, R.; Kumar, K. Impact of Urban Heat Island Formation on Energy Consumption in Delhi. *Urban Clim.* **2021**, *36*, 100763. [[CrossRef](#)]
84. Sharma, A.; Kumar, V.; Shahzad, B.; Tanveer, M.; Sidhu, G.P.S.; Handa, N.; Kohli, S.K.; Yadav, P.; Bali, A.S.; Parihar, R.D.; et al. Worldwide Pesticide Usage and Its Impacts on Ecosystem. *SN Appl. Sci.* **2019**, *1*, 1446. [[CrossRef](#)]
85. Sobrino, J.A.; Oltra-Carrió, R.; Sòria, G.; Bianchi, R.; Paganini, M. Impact of Spatial Resolution and Satellite Overpass Time on Evaluation of the Surface Urban Heat Island Effects. *Remote Sens. Environ.* **2012**, *117*, 50–56. [[CrossRef](#)]
86. Liu, Z.; Lai, J.; Zhan, W.; Bechtel, B.; Voogt, J.; Quan, J.; Hu, L.; Fu, P.; Huang, F.; Li, L.; et al. Urban Heat Islands Significantly Reduced by COVID-19 Lockdown. *Geophys. Res. Lett.* **2022**, *49*, e2021GL096842. [[CrossRef](#)]
87. San Martini, F.M.; Hasenkopf, C.A.; Roberts, D.C. Statistical Analysis of PM_{2.5} Observations from Diplomatic Facilities in China. *Atmos. Environ.* **2015**, *110*, 174–185. [[CrossRef](#)]
88. Sharma, R.; Pradhan, L.; Kumari, M.; Bhattacharya, P. Assessing Urban Heat Islands and Thermal Comfort in Noida City Using Geospatial Technology. *Urban Clim.* **2021**, *35*, 100751. [[CrossRef](#)]
89. Hong, J.; Lee, M.; Huh, W.; Kim, T.K.; Jeon, J.; Lee, H.; Kim, K.; Byeon, S.; Park, C.; Kim, H.S. Comparisons of PM_{2.5} Mitigation with Stand Characteristics between Evergreen Korean Pine Plantations and Deciduous Broad-Leaved Forests in the Republic of Korea. *Environ. Pollut.* **2023**, *334*, 122240. [[CrossRef](#)]
90. Lee, H.; Jeon, J.; Lee, M.; Kim, H.S. Seasonal Contrasting Effects of PM_{2.5} on Forest Productivity in Peri-urban Region of Seoul Metropolitan Area, Republic of Korea. *Agric. For. Meteorol.* **2022**, *325*, 109149. [[CrossRef](#)]
91. Chen, Y.; Ke, X.; Min, M.; Zhang, Y.; Dai, Y.; Tang, L. Do We Need More Urban Green Space to Alleviate PM_{2.5} Pollution? A Case Study in Wuhan, China. *Land* **2022**, *11*, 776. [[CrossRef](#)]
92. Yin, S.; Zhang, X.; Yu, A.; Sun, N.; Lyu, J.; Zhu, P.; Liu, C. Determining PM_{2.5} Dry Deposition Velocity on Plant Leaves: An Indirect Experimental Method. *Urban For. Urban Green.* **2019**, *46*, 126467. [[CrossRef](#)]

Disclaimer/Publisher’s Note: The statements, opinions and data contained in all publications are solely those of the individual author(s) and contributor(s) and not of MDPI and/or the editor(s). MDPI and/or the editor(s) disclaim responsibility for any injury to people or property resulting from any ideas, methods, instructions or products referred to in the content.